

A PP6-Type Phosphatase Holoenzyme Directly Regulates PIN Phosphorylation and Auxin Efflux in *Arabidopsis*

Mingqiu Dai,^a Chen Zhang,^{b,c,1} Urszula Kania,^{d,e,1} Fang Chen,^a Qin Xue,^a Tyra Mccray,^a Gang Li,^a Genji Qin,^f Michelle Wakeley,^{a,g} William Terzaghi,^{a,g} Jianmin Wan,^h Yunde Zhao,^f Jian Xu,^{b,c} Jiri Friml,^{d,e} Xing Wang Deng,^a and Haiyang Wang^{a,h,i,j,2}

^a Department of Molecular, Cellular, and Developmental Biology, Yale University, New Haven, Connecticut 06520-8104

^b National University of Singapore, Department of Biological Sciences, Singapore 117543

^c National Key Laboratory of Crop Genetic Improvement, Huazhong Agricultural University, Wuhan 430070, China

^d Department of Plant Systems Biology, VIB, Ghent University, 9052 Ghent, Belgium

^e Department of Plant Biotechnology and Genetics, Ghent University, 9052 Ghent, Belgium

^f Section of Cell and Developmental Biology, University of California–San Diego, La Jolla, California 92093-0116

^g Department of Biology, Wilkes University, Wilkes-Barre, Pennsylvania 18766

^h Institute of Crop Sciences, Chinese Academy of Agriculture Sciences, Beijing 100081, China

ⁱ Capital Normal University, Beijing 100048, China

^j National Engineering Research Center for Crop Molecular Design, Beijing 100085, China

The directional transport of the phytohormone auxin depends on the phosphorylation status and polar localization of PIN-FORMED (PIN) auxin efflux proteins. While PINIOD (PID) kinase is directly involved in the phosphorylation of PIN proteins, the phosphatase holoenzyme complexes that dephosphorylate PIN proteins remain elusive. Here, we demonstrate that mutations simultaneously disrupting the function of *Arabidopsis thaliana* *FyPP1* (for Phytochrome-associated serine/threonine protein phosphatase1) and *FyPP3*, two homologous genes encoding the catalytic subunits of protein phosphatase6 (PP6), cause elevated accumulation of phosphorylated PIN proteins, correlating with a basal-to-apical shift in subcellular PIN localization. The changes in PIN polarity result in increased root basipetal auxin transport and severe defects, including shorter roots, fewer lateral roots, defective columella cells, root meristem collapse, abnormal cotyledons (small, cup-shaped, or fused cotyledons), and altered leaf venation. Our molecular, biochemical, and genetic data support the notion that *FyPP1/3*, *SAL* (for SAPS DOMAIN-LIKE), and *PP2AA* proteins (*RCN1* [for ROOTS CURL IN NAPHTHYLPHTHALAMIC ACID1] or *PP2AA1*, *PP2AA2*, and *PP2AA3*) physically interact to form a novel PP6-type heterotrimeric holoenzyme complex. We also show that *FyPP1/3*, *SAL*, and *PP2AA* interact with a subset of PIN proteins and that for *SAL* the strength of the interaction depends on the PIN phosphorylation status. Thus, an *Arabidopsis* PP6-type phosphatase holoenzyme acts antagonistically with *PID* to direct auxin transport polarity and plant development by directly regulating PIN phosphorylation.

INTRODUCTION

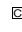
Auxin is a fundamental plant hormone that regulates almost every aspect of plant growth and development, including embryogenesis, organogenesis, apical dominance, tissue regeneration, and tropisms (reviewed in Bennett and Scheres, 2010; Grunewald and Friml, 2010; Peris et al., 2010). Auxin is transported from its sites of biosynthesis to its sites of action by a polarized auxin transport system. Molecular genetic studies in *Arabidopsis thaliana* have led to the identification and functional characterization of several key players of the polarized auxin transport system, such as the

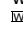
auxin uptake carriers AUXIN RESISTANT1/LIKE AUX1 (*AUX1*/*LAX*) (Swarup et al., 2008), the auxin efflux carriers, including PIN-FORMED (*PIN*) family proteins (Gälweiler et al., 1998; Chen et al., 1998; Müller et al., 1998; Friml et al., 2002; Petrásek et al., 2006), and P-glycoprotein auxin transporters *ABCB1* (for ATP BINDING CASSETTE PROTEIN SUBFAMILY B1), *ABCB4*, and *ABCB19* (Terasaka et al., 2005; Bouchard et al., 2006; Blakeslee et al., 2007; Lin and Wang, 2005). *PIN* proteins are asymmetrically targeted to the plant cell plasma membranes, resulting in distinct polar subcellular localization in a given tissue. For example, *PIN1* is localized in the basal (rootward, lower) plasma membrane of stele cells and xylem cells in the vascular system, which is required for long-distance auxin flow from the shoot apex to the root tip (Gälweiler et al., 1998; Friml et al., 2002). *PIN2* is expressed in root tissues and is selectively localized to the apical (shootward, upper) side of lateral root cap cells and epidermal cells (Müller et al., 1998; Kleine-Vehn et al., 2008). Polar localization of *PIN* proteins facilitates auxin flow and determines the direction of local intercellular auxin transport and subsequently regulates plant development (Wiśniewska et al., 2006).

¹ These authors contributed equally to this work.

² Address correspondence to haiyang.wang@yale.edu.

The author responsible for distribution of materials integral to the findings presented in this article in accordance with the policy described in the Instructions for Authors (www.plantcell.org) is: Haiyang Wang (haiyang.wang@yale.edu).

 Some figures in this article are displayed in color online but in black and white in the print edition.

 Online version contains Web-only data.

www.plantcell.org/cgi/doi/10.1105/tpc.112.098905

Substantial genetic and pharmacological evidence supports the involvement of phosphorylation in the regulation of PIN-dependent auxin transport polarity (Benjamins et al., 2001; Friml et al., 2004; Zhang et al., 2010; Huang et al., 2010). PINOID (PID), a Ser/Thr kinase, was reported to directly phosphorylate PIN proteins and thus to play an important role in mediating the polar targeting of PIN proteins. Loss of PID function causes an apical-to-basal shift in PIN polarity, while PID gain of function results in the opposite basal-to-apical shift in PIN polarity (Friml et al., 2004; Michniewicz et al., 2007; Huang et al., 2010). Altered PID activity causes changes in auxin flow, leading to severe defects in various developmental processes (Christensen et al., 2000; Benjamins et al., 2001; Friml et al., 2004). Besides PID, two other AGC3 kinases, including WAVY ROOT GROWTH1 (WAG1) and WAG2 were also reported to phosphorylate PIN proteins (Dhonukshe et al., 2010). Overexpression of PID, WAG1, or WAG2 leads to comparable root phenotypes, including root meristem collapse and agravitropic root growth, as a result of the basal-to-apical shift of PIN1, PIN2, and PIN4 localization (Dhonukshe et al., 2010).

Protein phosphorylation by kinases and dephosphorylation by phosphatases represent a major mechanism regulating eukaryotic cell signaling (Terol et al., 2002). Protein phosphatases can be classified into different groups based on their sequence, structure, and catalytic mechanism (Moorhead et al., 2007). In general, the PP2A heterotrimeric holoenzyme consists of a catalytic C subunit, a type A regulatory subunit, and a type B regulatory subunit (Terol et al., 2002). Whereas the A regulatory subunits are composed of tandem HEAT repeats that form a hook-like architecture for binding the catalytic and regulatory B subunits, and are hence also known as the scaffold subunits or structural subunits, the type B regulatory subunits of PP2A are diverse (Farkas et al., 2007; Janssens et al., 2008). The catalytic subunits of PP2A (PP2Ac), PP4 (PP4c), and PP6 (PP6c) are most closely related, based on their sequence homology (54 to 64% identities); therefore, they are considered to be PP2A-like phosphatases (Moorhead et al., 2007). However, the specificity of PP2Ac, PP4c, and PP6c function in vivo is derived from a group of regulatory subunits that are unique to their holoenzymes. For example, in mammals, PP2Ac associates with a scaffolding A- α or - β subunit and an additional regulatory B subunit to form the holoenzyme and gain its full activity, PP4c binds to four unique direct binding partners and other partners, and PP6c binds to the SAPS domain proteins and other binding partners, such as ankyrin repeat-containing proteins, to form PP6 holoenzyme and build up the activity specificity (Luke et al., 1996; G.I. Chen et al., 2008; Slupe et al., 2011). However, the in vivo holoenzyme composition and developmental roles of these phosphatases are still poorly understood in plants.

In *Arabidopsis*, the type A regulatory subunits of PP2A phosphatase (hereafter, PP2AAs, including PP2AA1, also known as RCN1 [for ROOTS CURL IN NAPHTHYLPHTHALAMIC ACID1], PP2AA2, and PP2AA3), were suggested to regulate PIN phosphorylation state and auxin transport (Garbers et al., 1996; Rashotte et al., 2001; Zhou et al., 2004; Michniewicz et al., 2007). In addition, it was recently reported that a phytochrome-associated Ser/Thr protein phosphatase, FyPP1, plays a role in regulating the interdigitated expansion pattern of leaf epidermis

cells by influencing PIN1 localization (Li et al., 2011). However, the phosphatase holoenzyme complex(es) responsible for directly interacting with and dephosphorylating PIN proteins still remains to be identified.

In this study, we show that mutations simultaneously disrupting the function of *Arabidopsis* *FyPP1* and its homologous gene *FyPP3* cause severe defects in a wide range of developmental processes, resulting in shorter roots, fewer lateral roots, defective columella cells, root meristem collapse, abnormal cotyledons (small, cup-shaped, or fused cotyledons), and altered leaf venation. We demonstrate that FyPP1 and FyPP3 interact with a subset of PIN proteins and regulate PIN protein phosphorylation and targeting in vivo. We further show that FyPP1 and FyPP3 also directly interact with SAL proteins and PP2AAs to form the PP6 heterotrimeric holoenzyme complex. Moreover, mutations simultaneously disrupting the function of four SAL genes also display developmental defects similar to the *fyp1 fyp3* double mutants and *pp2aa* higher order mutants. Our data support a model in which PP6 acts antagonistically with PID to regulate the reversible phosphorylation of PIN and polar targeting, subsequently impacting polar auxin transport and plant development.

RESULTS

Phenotypic Characterization of *FyPP1* and *FyPP3* Loss- and Gain-of-Function Mutants

In *Arabidopsis*, *FyPP1* (located on chromosome 1) and *FyPP3* (located on chromosome 3) encode the catalytic subunits of PP6. These two homologous proteins share 99% amino acid identity, with only three differences out of 303 amino acids, and they share a high level of sequence identity (54 to 57% identities) with the C subunits of PP2A (PP2Ac1-5) (Kim et al., 2002; Farkas et al., 2007; see Supplemental Figure 1, Supplemental References 1, and Supplemental Data Set 1 online). In vitro assays showed that in contrast with PP2A, which does not need a cation for its activity (Wang et al., 2007), FyPP3 requires Zn^{2+} for its activity (Kim et al., 2002; Wang et al., 2007; see Supplemental Figure 2A online). In addition, it was reported that Asp-84 (D84) is responsible for the enzyme activity of human PP6 (Kajino et al., 2006). We thus identified the homologous Asp residues in FyPP1 and FyPP3 (D81) and mutated them into Asn (N) residues (FyPP1^{D81N} and FyPP3^{D81N}). In vitro analyses indicated that the mutant phosphatase lost almost all activity (see Supplemental Figure 2B online), supporting that these amino acids are indeed required for the activity of FyPP1 and FyPP3.

To investigate the role of *FyPP1* and *FyPP3* in plant developmental processes, we isolated T-DNA insertion mutants of *FyPP1* (*fyp1*) and *FyPP3* (*fyp3*) (see Supplemental Figure 3 online). Single mutants of either *fyp1* (*f1*, hereafter) or *fyp3* (*f3*, hereafter) did not show significant phenotypic differences compared with wild-type plants, indicating a likely functional redundancy between *FyPP1* and *FyPP3*. By contrast, the *fyp1 fyp3* (hereafter, *f1 f3*) double mutant seedlings displayed a wide range of developmental defects, including shorter roots, fewer lateral roots, defective columella cells, root meristem collapse,

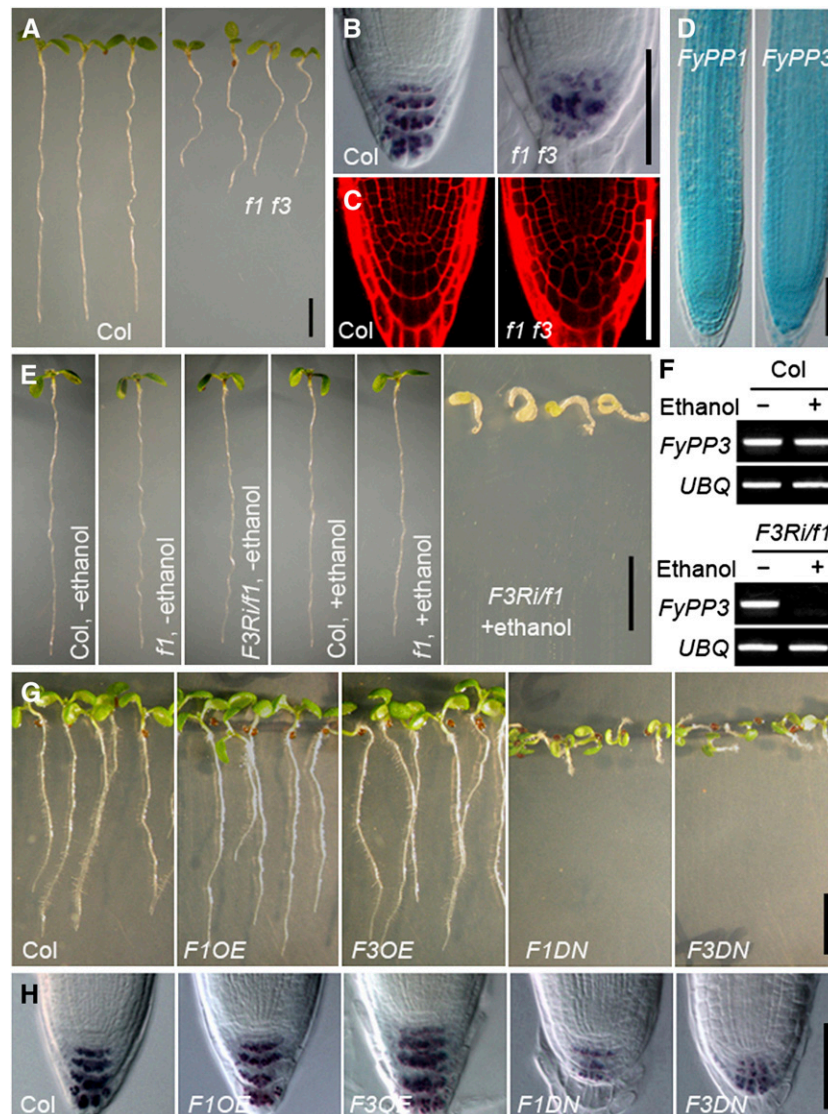


Figure 1. Phenotypic Characterization of Root Development in *f1 f3*, *F3Ri/f1*, *F1OE*, *F3OE*, *F1DN*, and *F3DN* Plants.

- (A) Shorter roots of *f1 f3* double mutants versus the Col wild type. Seedlings are shown at 5 DAG. Bar = 0.5 cm.
- (B) Reduced and more diffuse staining of starch granules in the root tips of *f1 f3* mutants, as indicated by Lugol's staining. Bar = 50 μ m.
- (C) Propidium iodide staining shows irregular cell arrangement and defective columella cells in the root tips of *f1 f3* mutants. Bar = 50 μ m.
- (D) GUS staining shows overlapping expression patterns of *FyPP1pro:GUS* and *FyPP3pro:GUS* in primary roots. Bar = 50 μ m.
- (E) Developmental defects of *FyPP3RNAi/fypp1* (*F3Ri/f1*) seedlings upon induction with ethanol. Bar = 1 cm.
- (F) Silenced expression of *FyPP3* gene in *F3Ri/f1* plants after ethanol induction shown in (E).
- (G) *F1OE* and *F3OE* roots are slightly longer than Col roots, while *F1DN* and *F3DN* roots exhibit reduced root length and agravitropism compared with Col. Seedlings are shown at 5 DAG. Bar = 1 cm.
- (H) Lugol's staining showing that the staining of starch granules is dramatically reduced in the root tips of *F1DN* and *F3DN* roots, while the staining of starch granules is largely normal in *F1OE* and *F3OE* roots compared with Col. Bar = 50 μ m.

abnormal cotyledons (small, cup-shaped, or fused cotyledons), and altered leaf venation (Figures 1A to 1C; see Supplemental Figures 4A to 4E online). Consistent with the root phenotypes, histochemical staining of *FyPP1pro:GUS* (for β -glucuronidase) and *FyPP3pro:GUS* transgenic plants showed that both *FyPP1* and *FyPP3* were ubiquitously expressed in the root (Figure 1D).

Since the *f3* mutant retains a truncated form of *FyPP3* (*FyPP3 Δ*) (see Supplemental Figure 3 online), which may have partial *FyPP3* function, we generated several ethanol-inducible RNA interference (RNAi) lines for *FyPP3* in the *f1* mutant background (*F3Ri/f1*, hereafter). Without ethanol induction, the *F3Ri/f1* seedlings did not show any visible phenotypic changes

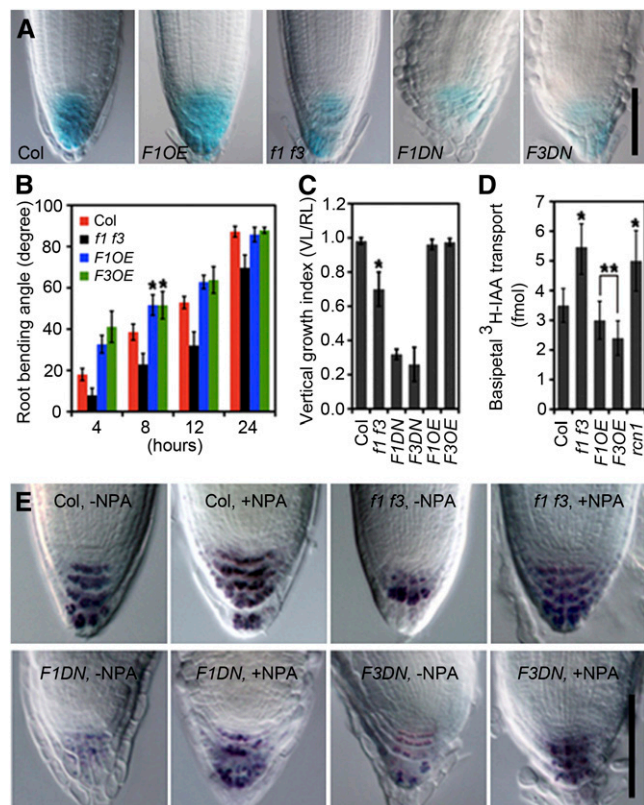


Figure 2. Characterization of Auxin-Related Root Developmental Processes in *f1 f3*, *F1OE*, *F3OE*, *F1DN*, and *F3DN* Transgenic Plants.

(A) *DR5:GUS* activity is reduced in *f1 f3*, *F1DN*, and *F3DN* roots but normal in the *F1OE* roots compared with Col. Twenty plants were used in each GUS staining experiment, with three replicates.

(B) *f1 f3* mutant roots are less sensitive, while *F1OE* and *F3OE* roots are more sensitive to gravistimulation than Col at different time points after reorientation (4, 8, 12, and 24 h).

(C) Roots of *f1 f3*, *F1DN*, and *F3DN* transgenic plants exhibit reduced vertical growth indices (VGI = vertical length [VL]/root length [RL]) at 5 DAG.

(D) The root auxin basipetal transport is enhanced in *f1 f3* roots, while slightly reduced in *F1OE* and *F3OE* roots, compared with Col. *rcn1* was used as a positive control.

(E) NPA largely restores the starch staining pattern in *f1 f3*, *F1DN*, and *F3DN* root tips. Twenty plants were used in each Lugol's staining experiment, with three replicates.

Error bars represent \pm SE; $n = 20$. Asterisks indicate the levels of statistical significance as determined by Student's *t* test: * $P < 0.001$ and ** $P < 0.04$ versus Col; $n \geq 20$. Bars = 50 μ m in **(A)** and **(E)**.

compared with the *f1* single mutants or wild-type controls (Columbia [Col]); however, after ethanol induction, the *F3Ri/f1* seedlings exhibited developmental defects similar to or even more severe than those of the *f1 f3* double mutant, including dramatically shortened primary roots and defective gravitropism (Figure 1E; see Supplemental Figure 4F online). Gene expression analysis showed that expression of *FyPP3* in *F3Ri/f1* seedlings was silenced after ethanol induction, whereas ethanol itself had no obvious effect on the expression of *FyPP3* (Figure 1F),

indicating that the developmental defects in *F3Ri/f1* seedlings after ethanol induction were specifically associated with silenced expression of *FyPP3*.

To further investigate the function of *FyPPs* in plant development, we generated transgenic *Arabidopsis* plants overexpressing *FyPP1* or *FyPP3* (see Supplemental Figures 5A and 5B online). We observed that both *35S:YFP-FyPP1/Col* (hereafter, *F1OE*; YFP for yellow fluorescent protein) and *35S:YFP-FyPP3/Col* (hereafter, *F3OE*) seedlings had longer primary roots than wild-type seedlings (Figure 1G; see Supplemental Figure 6B online), although the root tip structure of the overexpressors was essentially normal (Figure 1H). Thus, *FyPP* overexpressors displayed a phenotype partially opposite to that of the *f1 f3* double mutants and *F3Ri/f1* plants induced with ethanol.3

Phenotypic Characterization of *FyPP1* and *FyPP3* Dominant-Negative Mutants

To address the impact of PP6 phosphatase-null variants on the plant growth, we generated transgenic *Arabidopsis* plants overexpressing the *D81N* mutant forms of *FyPP1* (*35S:YFP-FyPP1^{D81N}/Col*; hereafter, *F1DN*) and *FyPP3* (*35S:YFP-FyPP3^{D81N}/Col*; hereafter, *F3DN*) (see Supplemental Figures 5C and 5D online). Interestingly, the proteins of YFP-*FyPP1^{D81N}* in *F1DN* and YFP-*FyPP3^{D81N}* in *F3DN* accumulated to a much higher level than YFP-*FyPP1* in *F1OE* and YFP-*FyPP3* in *F3OE* lines (see Supplemental Figures 5E to 5I online) despite their comparable mRNA accumulation (see Supplemental Figure 5J online), indicating that D81 is not only the PP6 active site, but also responsible for the stability of *FyPP1* and *FyPP3* proteins. Genetic complementation analysis showed that YFP-*FyPP1*, but not YFP-*FyPP1^{D81N}*, fully rescued the *f1 f3* mutant root phenotypes (see Supplemental Figure 6A online), indicating that the YFP-*FyPP1* fusion protein is biologically functional. Notably, we observed that both *F1DN* and *F3DN* seedlings had significantly shorter primary roots and a much weaker Lugol's staining pattern at the root tip than wild-type seedlings (Figures 1G and 1H; see Supplemental Figure 6B online). Most strikingly, the *F1DN* and *F3DN* seedlings were totally agravitropic (Figure 1G), which is similar to the *pp2aa* loss-of-function mutants (Michniewicz et al., 2007) or *PID*, *WAG1*, and *WAG2* gain-of-function mutants (Benjamins et al., 2001; Dhonukshe et al., 2010). The agravitropic root growth phenotype was also observed in the *F1DN* and *F3DN* seedlings at 10 d after germination (DAG) (see Supplemental Figure 6C online). These observations indicated that overexpression of the *D81N* mutant forms of *FyPP1* and *FyPP3* caused a pleiotropic phenotype more severe than that of the *f1 f3* double mutant but comparable with that of the *F3Ri/f1* seedlings following ethanol treatment. Together, these data suggest that *FyPP1* and *FyPP3* play a critical role in regulating a broad range of plant developmental processes and that the *FyPP1^{D81N}* and *FyPP3^{D81N}* mutants most likely regulate plant development in a dominant negative fashion.

In general, the range of root and cotyledon defects in different *FyPP* loss-of-function mutants was strongly reminiscent of the defects reported for auxin signaling mutants, such as *mp* (Schlereth et al., 2010) and *wax1* (Ge et al., 2010), or auxin transport mutants, such as mutants defective in multiple PIN

auxin transporters (Friml et al., 2003; Blilou et al., 2005), or *pp2aa* loss- and *PID* gain-of-function mutants that are defective in PIN polar localization (Friml et al., 2004; Michniewicz et al., 2007).

FyPP1 and FyPP3 Are Required for Polar Auxin Transport

Phenotypic characterization of the *FyPP* loss-of-function mutants and overexpression lines suggested that many of the altered developmental processes were related to developmental processes regulated by auxin. To investigate this further, we examined the activity of an auxin response reporter, *DR5:GUS* (Ulmasov et al., 1997), in the root tips of *Col*, *F1OE*, *f1 f3*, *F1DN*, and *F3DN* plants. GUS signal was much lower in the *f1 f3*, *F1DN*, and *F3DN* roots compared with *Col* but not in the *F1OE* roots (Figure 2A), indicating that auxin responses and/or auxin transport were indeed affected in the *FyPP* loss-of-function plants.

We also examined the responses of *f1 f3*, *F1OE*, and *F3OE* plants to exogenously applied auxin. When treated with the synthetic auxins 2,4-D or naphthalene-1-acetic acid, elongation of wild-type, *f1 f3*, *F1OE*, and *F3OE* roots was similarly inhibited (see Supplemental Figure 7A online). We also observed comparable induction of *DR5* activity in wild-type, *f1 f3*, *F1OE*, and *F3DN* plants after indole-3-acetic acid (IAA) treatment (see Supplemental Figure 7B online). These data suggested that auxin responses are relatively normal in plants with altered *FyPP1/FyPP3* function.

Root bending in response to gravity is a typical adaptation growth response dependent on regulated polar movement of auxin (Swarup et al., 2005). To study the potential role of *FyPPs* in gravitropism, we used a root-bending assay to investigate the responses of *f1 f3*, *F1OE*, and *F3OE* seedlings to gravistimulation. We observed that the *f1 f3* double mutants showed a delayed response to gravistimulation compared with *Col* plants, while the *F1OE* and *F3OE* plants showed a hyperbending response to

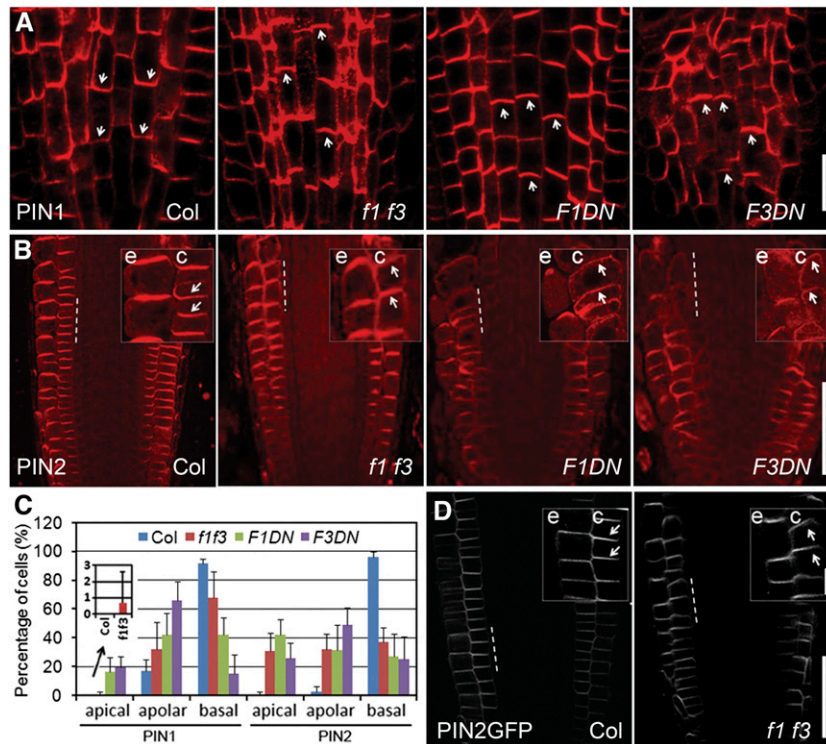


Figure 3. Altered PIN1 and PIN2 Localization in the Roots of *f1 f3*, *F1DN*, and *F3DN* Mutants.

(A) Immunolocalization of PIN1 in 6-DAG roots. PIN1 polar localization is disturbed, with visible apicalization in some stele cells of *f1 f3*, *F1DN*, and *F3DN* roots compared with the basal localization of PIN1 in *Col*.

(B) Immunolocalization of PIN2 in 6-DAG roots. In the *Col* background, PIN2 was localized to the upper side of the epidermal cells and the lower side of the cortical cells but shifted from basal to apical sides in the cortex of *f1 f3*, *F1DN*, and *F3DN* roots.

(C) Percentage of cells with apical, apolar, or basal localization of PIN1 (in stele cells) or PIN2 (in cortical cells) in *Col*, *f1 f3*, *F1DN*, and *F3DN* roots. The imbedded image is an enlarged view of the columns showing percentage of stele cells with PIN1 apical localization in *Col* and *f1 f3* roots. Error bars represent SE; *n* = 10.

(D) Changed PIN2-GFP localization in 6-DAG *f1 f3* roots: basal-to-apical shift of PIN2-GFP signal in the *f1 f3* cortex compared with the basal localization of PIN2-GFP in cortical cells of *Col*.

Enlarged views of the indicated areas (by dashed lines) in **(B)** and **(D)** are shown at the top right side of each panel, respectively. c, cortex; e, epidermis. Arrowheads indicate polarity of PIN localization. Bars = 50 μm in **(A)**, **(B)**, and **(D)** and 10 μm in the enlarged views in **(B)** and **(D)**.

gravistimulation (Figure 2B). Similarly, the root vertical growth index confirmed the root gravitropic defect in the *f1 f3* double mutant and the *F1DN* and *F3DN* lines (Figure 2C). These observations suggested that auxin transport is altered in the *f1 f3* double mutant and in the *F1DN*, *F3DN*, *F1OE*, and *F3OE* lines.

To confirm a role for *FyPP1* and *FyPP3* in auxin transport, we measured the uptake of ^3H -labeled IAA in the roots of *f1 f3* mutants and *F1OE* and *F3OE* lines. Root basipetal auxin transport was enhanced in *f1 f3* mutants but slightly suppressed in *F1OE* and *F3OE* plants (Figure 2D). We were unable to directly measure auxin transport in the roots of *F1DN* and *F3DN* transgenic lines due to their extremely short roots and disrupted root structure. In addition, we observed that the auxin transport inhibitor 1-*N*-naphthylphthalamic acid (NPA) could similarly inhibit the root basipetal auxin transport in Col and *f1 f3* roots (see Supplemental Figure 8 online) and largely correct the root tip defects of the *f1 f3* mutant and the *F1DN* and *F3DN* lines (Figure 2E), further supporting the notion that *f1 f3*, *F1DN*, and *F3DN* mutants are mainly affected in auxin transport.

FyPP1 and *FyPP3* Are Required for PIN Protein Polar Localization

The phenotype similarity between *FyPP* mutants and mutants with defective PIN polar localization (Benjamins et al., 2001; Michniewicz et al., 2007), and the localization of YFP-*FyPP1* and YFP-*FyPP3* proteins to the plasma membrane of the root cells (see Supplemental Figure 9 online) prompted us to test whether *FyPP1* and *FyPP3* are required for proper PIN localization. We performed immunolocalization of PIN1 and PIN2 in *f1 f3*, *F1DN*, and *F3DN* mutants. In Col roots, PIN1 is localized to the basal side in the stele cells (Blilou et al., 2005; Figure 3A) and PIN2 is localized to the apical side in epidermal and to the basal side in cortical cells (Friml et al., 2004; Figure 3B), whereas in the *f1 f3*, *F1DN*, and *F3DN* roots, there is a switch from basal to apical

localization for PIN1 in the stele cells (Figure 3A) and for PIN2 in the cortical cells (Figure 3B), although the apical localization of PIN2 in epidermal cells was not affected (Figure 3B). Statistical analysis showed that, compared with the Col wild type, more stele cells showed disrupted PIN1 polar localization and more cortical cells showed disrupted PIN2 polar localization (with apical or apolar localization) in *f1 f3*, *F1DN*, and *F3DN* roots (Figure 3C). We also crossed a *PIN2pro:PIN2-GFP* (for green fluorescent protein) reporter gene into the *f1 f3* mutant background. As expected, we observed a basal-to-apical shift of PIN2-GFP in the cortical cells of *f1 f3* roots, although the apical localization of PIN2-GFP appears to be normal in epidermal cells of *f1 f3* roots (Figure 3D). Taken together, these observations indicate that *FyPP1* and *FyPP3* are required for proper PIN polar localization to the basal side of cells and loss of their activity leads to a basal-to-apical shift in PIN targeting.

FyPP1 and *FyPP3* Directly Dephosphorylate PIN Proteins

We next examined whether phosphorylation of PIN proteins is affected in plants with altered PP6 activity using the hydrophilic loops (HLs) of PIN2 as the substrate (Michniewicz et al., 2007; Dhonukshe et al., 2010). Equal amounts of recombinant HIS-PIN2HL proteins were coincubated separately with equal amounts of extracts prepared from wild-type, *f1 f3* mutant, *PID-OE*, *F1DN*, and *F1OE* transgenic plants in an *in vitro* phosphorylation assay. The amounts of phosphorylated PIN2HL were higher in samples treated with protein extracts from *f1 f3*, *F1DN*, and *PID-OE* transgenic plants, but not with protein extracts from *F1OE* plants, compared with Col (Figure 4A). These data indicate that the protein extracts derived from plants that lack PP6 activity, such as *f1 f3* and *F1DN* mutants, have reduced abilities to dephosphorylate PIN2HL. To confirm our conclusion, we grew *F3Ri/f1* seedlings on germination media (GM) plates for 3 d and then transferred these seedlings to fresh

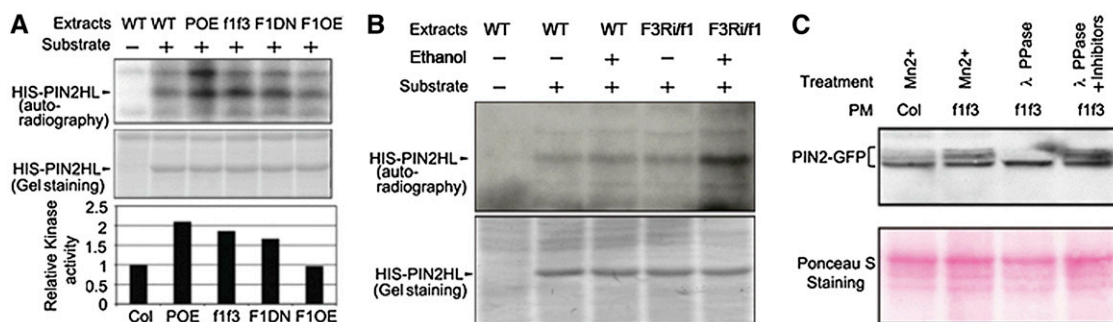


Figure 4. PP6-Dependent Dephosphorylation of PIN Proteins.

(A) *In vitro* kinase assay shows that the abundance of phosphorylated HIS-PIN2HL is higher when treated with plant extracts derived from *PID-OE* (*POE*), *f1 f3*, and *F1DN* seedlings compared with the treatments with plant extracts derived from Col and *F1OE* seedlings. WT, the wild type.

(B) *In vitro* kinase assay shows that the abundance of phosphorylated HIS-PIN2HL is higher when treated with plant extracts derived from *F3Ri/f1* seedlings induced by ethanol than when treated with plant extracts derived from Col seedlings with or without ethanol induction and *F3Ri/f1* seedlings without ethanol induction.

(C) Increased accumulation of higher molecular weight PIN2-GFP bands in *f1 f3* roots compared with Col. These bands are sensitive to λ -phosphatase treatment but stable in the presence of phosphatase inhibitors. Mn^{2+} was added to each reaction to make the reaction buffer comparable. Ponceau S staining shows the loading control. PM, plasma membrane.

[See online article for color version of this figure.]

GM plates with or without ethanol for another 3 d, when *F3Ri/f1* seedlings showed agravitropic growth after ethanol induction (see Supplemental Figure 10 online). In vitro phosphorylation assay showed that the amounts of phosphorylated PIN2HL were obviously higher in the sample treated with protein extracts from

F3Ri/f1 plants induced by ethanol but not in the samples treated with protein extracts from *F3Ri/f1* plants without ethanol induction or Col seedlings with or without ethanol treatment (Figure 4B). To test whether FyPP1/3 dephosphorylates PIN2 in vivo, we compared the migration of PIN2-GFP from Col and *f1 f3*

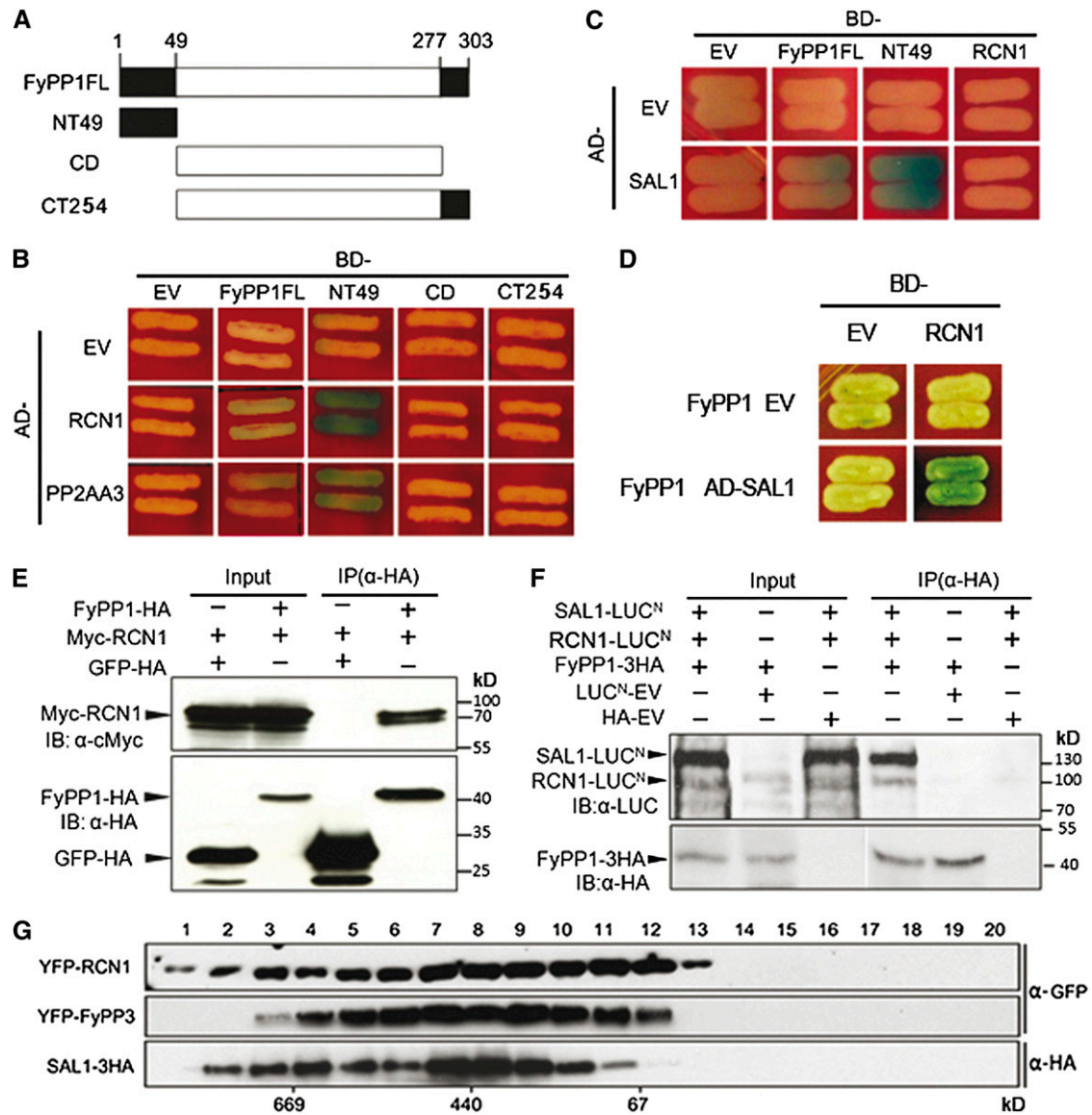


Figure 5. Protein-Protein Interactions among FyPP, PP2A, and SAL1.

(A) Schematic representation of the domain structure of FyPP1 used in the yeast two-hybrid assays. CD, catalytic domain; CT254, C-terminal region (amino acids 50 to 303); FL, full length; NT49, N-terminal region (amino acids 1 to 49).

(B) FyPP1 interacts with RCN1 and PP2A A3 in yeast cells. AD, B42 activation domain; BD, LexA DNA binding domain; EV, empty vector.

(C) SAL1 interacts with FyPP1, but not RCN1 in yeast cells.

(D) FyPP1 is required for the interaction between SAL1 and RCN1 in a yeast three-hybrid assay.

(E) In vivo coimmunoprecipitation of FyPP1 and RCN1. An α-HA affinity matrix was used for immunoprecipitation (IP); α-HA and α-Myc anti-bodies were used for immunoblotting (IB).

(F) In vivo coimmunoprecipitation of FyPP1, RCN1, and SAL1. An α-HA affinity matrix was used for immunoprecipitation, and α-HA and α-LUC anti-bodies were used for immunoblotting.

(G) Gel filtration assay shows that RCN1, SAL1, and FyPP3 are present in the same protein complex(es) in vivo. Fraction numbers are indicated on the top and molecular masses are indicated below the blot.

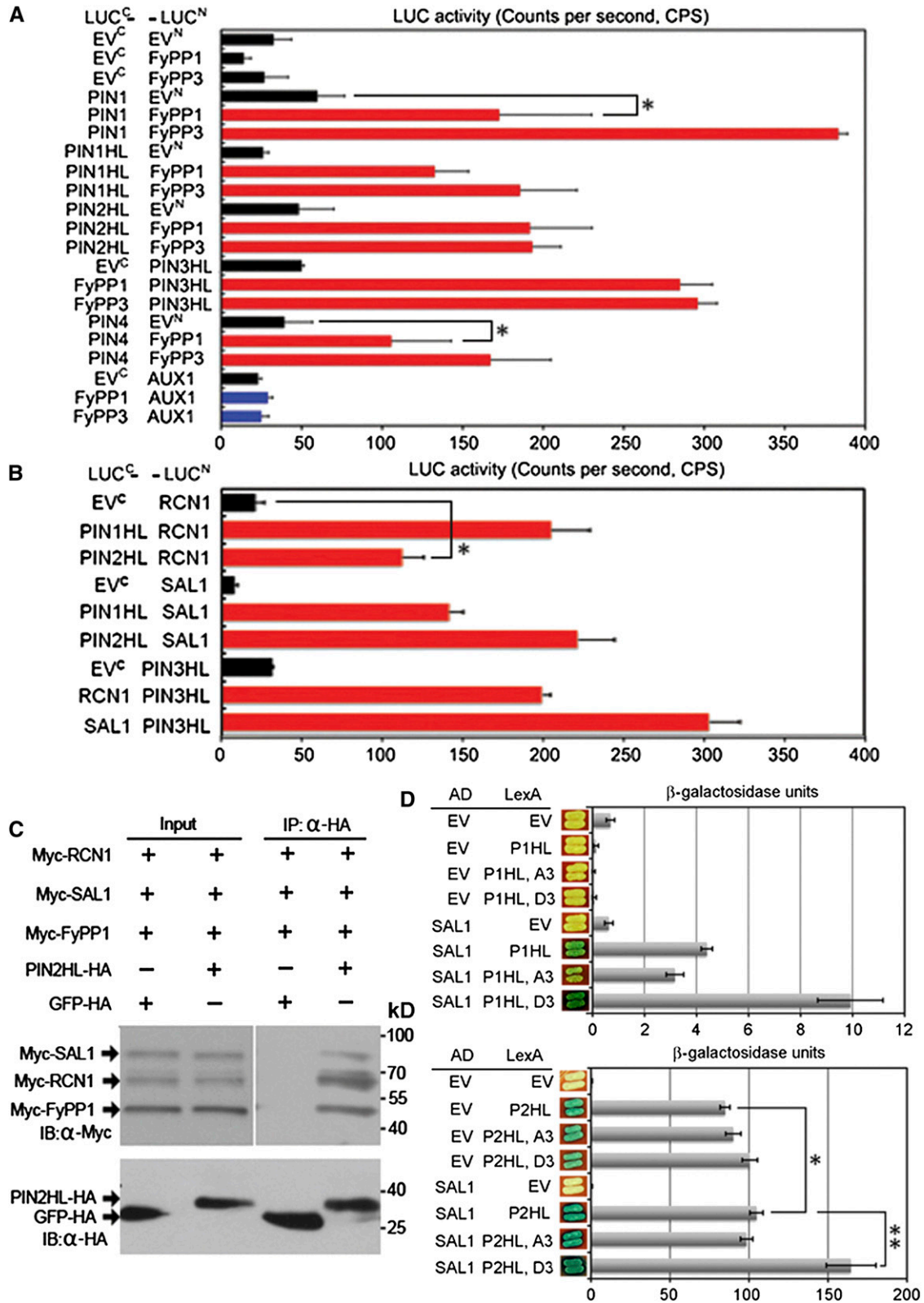


Figure 6. Protein-Protein Interactions among FyPP, PP2AA, SAL, and PIN Proteins.

backgrounds on SDS-PAGE gels. We observed more accumulation of the slowly migrating forms of PIN2-GFP (presumably phosphorylated isoforms) in *f1 f3* extracts (Figure 4C). These bands were sensitive to λ -phosphatase treatment but stable in the presence of phosphatase inhibitors (Figure 4C). These data further support the notion that dephosphorylation of PIN2-GFP in vivo is dependent on FyPP1 and FyPP3 activity.

FyPP, SAL, and the PP2AA Proteins Interact to Form the PP6 Heterotrimeric Holoenzyme

Considering the high sequence similarities among FyPP1, FyPP3, and PP2Ac1-5 (Kim et al., 2002; see Supplemental Figure 1 online) and the similar phenotypes of PP2AAs and FyPPs loss-of-function mutants, we reasoned that PP2AAs may also serve as the A regulatory subunits of PP6. In addition, it is known that SAPS domain proteins are the type B regulatory subunits of PP6 in humans (Stefansson and Brautigan, 2006). Homology searches identified four *Arabidopsis* SAPS domain-like proteins (SAL1-4), which share 45 to 72% sequence similarity. The Arabidopsis Information Resource public database shows that SAL proteins are located in either the plasma membrane or the endomembrane system (<http://www.Arabidopsis.org/>), which is similar to the subcellular localization of PP2AAs (Michniewicz et al., 2007; Blakeslee et al., 2008) and the membrane localization of FyPPs (see Supplemental Figure 9 online). We examined protein-protein interactions between these subunits in yeast and plants. Yeast two-hybrid (Y2H) assays showed that both PP2AAs (RCN1 and PP2AA3) and SAL1 directly interacted with FyPP1, and the N-terminal region of FyPP1 is responsible for these interactions (Figures 5A to 5C). Interestingly, we observed that FyPP1 was necessary for the interaction between RCN1 and SAL1 in a yeast three-hybrid assay (Figures 5C and 5D), suggesting that FyPP1, RCN1, and SAL1 could form a protein complex in yeast cells. Furthermore, in vivo coimmunoprecipitation assays showed that RCN1 coimmunoprecipitated with FyPP1 (Figure 5E) and that SAL1 and RCN1 together coimmunoprecipitated with FyPP1 in plant cells (Figure 5F). A gel filtration assay also showed that YFP-RCN1, SAL1-HA, and YFP-FyPP3 proteins were most abundant in the fractions around 440 kD (Figure 5G), which is consistent with the size of the previously purified human PP6 holoenzyme (Stefansson

et al., 2008). These results further confirmed that FyPP1 (or 3), RCN1, and SAL1 interact with each other to form a PP6-type phosphatase holoenzyme in vivo.

FyPP, SAL, and the PP2AA Proteins Interact with a Subset of PIN Proteins

To test whether PIN proteins may serve as the direct substrates of PP6 phosphatase, we performed a luciferase complementation assay (LCI) to check the interactions between PIN and FyPP1, RCN1, or SAL1. We observed that PIN1, PIN2, PIN3, and PIN4, but not AUX1 (which is an auxin influx carrier), interacted with both FyPP1 and FyPP3 in plant cells (Figure 6A). In addition, RCN1 interacted with PIN1, PIN2, and PIN3 at the HL (Figure 6B). We also observed the interactions between SAL1 and PIN1, PIN2, or PIN3 in plant cells (Figure 6B). These observations suggest that at least a subset of PIN proteins is the direct substrate of PP6 holoenzyme phosphatase. Further, in vivo coimmunoprecipitation assays showed that PIN2HL coimmunoprecipitated with RCN1, SAL1, and FyPP1 in plant cells (Figure 6C), and a bimolecular fluorescence complementation assay (BiFC) assay showed that FyPP3 interacted with both PIN1 and PIN2 at the membrane of onion (*Allium cepa*) cells (see Supplemental Figure 11 online). Taken together, these observations support the claim that PIN proteins are the direct targets of PP6 holoenzyme phosphatase activities.

It was reported that the Ser residues in PIN evolutionarily conserved TPRxS(N/S) motifs in the HLs are direct targets of AGC3 kinases and play critical roles in regulating proper PIN localization and auxin transport (Dhonukshe et al., 2010; Huang et al., 2010). To test whether these amino acid residues are involved in the interaction between PP6 and PIN1 or PIN2, we conducted site-directed mutagenesis to convert Ser into the nonphosphorylatable residue Ala (PIN1HL, A3; PIN2HL, A3) or into the phosphorylation-mimic Asp (PIN1HL, D3; PIN2HL, D3). We performed Y2H assays to investigate the interactions between various PIN HL proteins and SAL1. As shown in Figure 6D, the phosphorylation-mimic mutation of PIN1HL (P1HL, D3) and PIN2HL (P2HL, D3) enhanced the interaction between PIN1HL and SAL1 or PIN2HL and SAL1, respectively. These data suggest that these Ser sites are critical for mediating the interaction between PIN and PP6 and indicate a role for SAL1 in determining the substrate specificity of PP6.

Figure 6. (continued).

- (A)** LCI assays showing that both FyPP1 and FyPP3 interacted with PIN1, PIN2, PIN3, and PIN4 but not AUX1 in plant cells. Error bars represent SE; $n = 6$. Pairs for Student's *t* test are indicated with brackets; * $P < 0.01$.
- (B)** LCI assays showing that both RCN1 and SAL1 interacted with PIN1HL, PIN2HL, or PIN3HL in plant cells. Error bars represent SE; $n = 6$. Pairs for Student's *t* test are indicated with brackets; * $P < 0.01$.
- (C)** In vivo coimmunoprecipitation of FyPP1, RCN1, SAL1, and PIN2HL. An α -HA affinity matrix was used for immunoprecipitation (IP), and α -HA and α -Myc anti-bodies were used for immunoblotting (IB).
- (D)** Yeast X-Gal plate assay and β -galactosidase liquid assays showing that SAL1 interacted with various forms of the PIN1 HL (P1HL) or PIN2HL (P2HL) in yeast cells. Compared with the wild-type PIN HL, the phosphorylation mimic mutation of P1HL (P1HL-D3) enhanced the interaction between P1HL and SAL1 and the phosphorylation mimic mutation of P2HL (P2HL-D3) enhanced the interaction between P2HL and SAL1. P1HL-A3 and P2HL-A3 are the dephosphorylation mimic mutations of P1HL and P2HL, respectively. Error bars represent SE; $n = 3$ (pairs for Student's *t* test are indicated with brackets; * $P < 0.01$ and ** $P < 0.001$). AD, B42 activation domain; EV, empty vector; LexA, LexA DNA binding domain.

SAL Genes Are Required for Root Development and Proper PIN Polar Localization

To gain genetic evidence for the role of *SAL* genes in regulating auxin transport and root development, we isolated *sal1*, *sal2*, *sal3*, and *sal4* loss-of-function mutants (see Supplemental Figures 12A and 12B online). We did not observe significant phenotypic changes in *sal1*, *sal2*, *sal3*, and *sal4* single mutant seedlings compared with Col (see Supplemental Figure 12C online), indicating that there is probably functional redundancy among the members of the *SAL* gene family. However, transgenic plants overexpressing *SAL1* (*35S:SAL1-3HA/Col*; *SAL1-OE*, hereafter; see Supplemental Figure 12D online) had much longer roots than Col (see Supplemental Figures 12E and 12F online), suggesting a role for *SAL1* in regulating root development.

To further understand the role of *SAL* genes in plant development, we used an ethanol-inducible artificial microRNA (amiRNA) approach to simultaneously silence multiple *SAL* genes (Schwab et al., 2006; Michniewicz et al., 2007). We designed an amiRNA (amiR-SAL) to silence the expression of *SAL1*, *SAL3*, and *SAL4* and introduced this amiR-SAL into the *sal2* mutant background (*AlcA-AlcR:amiR-SAL/sal2* or *ARS2*, hereafter). We observed that after ethanol induction, *ARS2* seedlings had shorter roots than Col and exhibited agravitropic root growth (Figures 7A to 7C). Expression of *SAL1*, *SAL3*, and *SAL4* was dramatically inhibited in the *ARS2* lines after ethanol induction (Figure 7D), suggesting that the root development

defects of *ARS2* plants after ethanol induction are specifically associated with altered expression of the *SAL* genes.

To further test whether the *SAL* genes are involved in regulating PIN protein phosphorylation and targeting, we conducted an *in vitro* phosphorylation assay. We grew *ARS2* seedlings on GM plates for 3 d and then transferred these seedlings to fresh GM plates with or without ethanol for another 3 d, when *ARS2* seedlings showed agravitropic root growth after ethanol induction (see Supplemental Figures 13A and 13B online). We observed that the amounts of phosphorylated PIN2HL increased in the sample treated with protein extracts from *ARS2* plants induced by ethanol but not in the samples treated with protein extracts from *ARS2* plants without ethanol induction or Col seedlings with or without ethanol treatment (see Supplemental Figure 13C online). Immunostaining assays showed that, similar to the observations in *PP2AAs* loss-of-function mutants (Michniewicz et al., 2007), *f1 f3*, *F1DN*, and *F3DN* mutants (Figure 3), PIN1 localization has a basal-to-apical switch in the stele cells in *ARS2* roots (Figure 7F) compared with its basal localization in Col (Figure 7E). In addition, more PIN2 was localized to the apical side in the cortical cells in *ARS2* roots (Figure 7H) compared with the basal localization in the cortical cells in Col roots (Figure 7G), although its apical localization was not affected in epidermal cells in *ARS2* roots compared with Col (Figures 7G and 7H). These observations suggest that, like *PP2AAs* (Michniewicz et al., 2007) and *FyPPs*, *SALs* also regulate root development by regulating PIN phosphorylation and polar targeting.

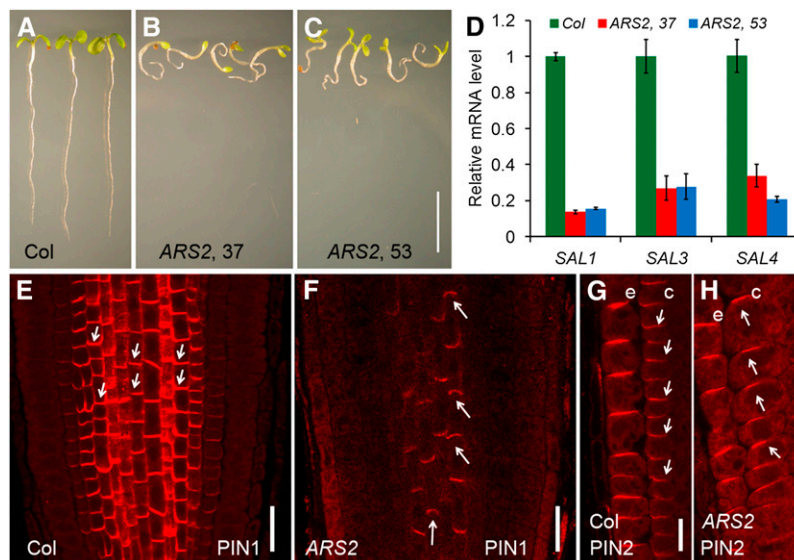


Figure 7. Defective PIN1 and PIN2 Localization in the Roots of Ethanol-Induced *ARS2* Transgenic Plants.

(A) to (C) After ethanol treatment, *ARS2* transgenic plants ((B) and (C)) had shorter roots and agravitropic root growth as compared with Col (A). (D) Dramatically reduced expression of *SAL1*, *SAL3*, and *SAL4* mRNA in *ARS2* lines after ethanol induction. Error bars represent SE; $n = 3$. (E) and (F) Immunolocalization of PIN1 in the 6-DAG roots of *ARS2* lines after ethanol induction. PIN1 polar localization was disturbed, with visible apicalization in some stele cells of *ARS2* roots compared with the basal localization of PIN1 in Col. (G) and (H) Immunolocalization of PIN2 in 6-DAG roots of *ARS2* lines after ethanol induction. In the Col background, PIN2 was localized to the upper side of the epidermal cells and the lower side of the cortical cells but shifted from basal to apical in the cortex of *ARS2* roots. e, epidermal cells; c, cortical cells. Arrows indicate polarity of PIN localization. Bars = 2 cm in (A) to (C), 50 μm in (E) and (F), and 20 μm in (G) and (H).

PP6 Acts Antagonistically with PID to Regulate Plant Development

To further test the genetic interactions between *FyPPs* and *RCN1* and *SAL1*, we introduced the *f1 f3* mutation into the *rcn1-6* (Blakeslee et al., 2008) and *sal1* mutant backgrounds. Both *rcn1 f1 f3* and *sal1 f1 f3* triple mutants had shorter roots than their parental lines (Figure 8A). Notably, the *rcn1 f1 f3* triple mutants were almost completely agravitropic, whereas *rcn1 f1^{-/+} f3* seedlings showed reduced sensitivity to gravity compared with their parental lines (Figure 8B). Considering that *f1^{-/+} f3* (*f1* is heterozygous and *f3* is homozygous) seedlings did not show significant phenotypic changes, this result suggests that *f1* and *f3* have a dosage effect on the phenotype of *rcn1*. In addition, we observed that *sal1 f1 f3* triple mutant seedlings showed a reduced sensitivity to gravity and the phenotype was much more severe than the parental plants (Figure 8B). These observations suggest that *FyPPs*, *PP2AAs*, and *SALs* function synergistically to regulate plant development.

To investigate the genetic interactions between *PP6* and *PID*, we introduced *35S:PID-GFP (PID-OE)* into *f1 f3*, *F1DN*, and *F3DN* backgrounds by genetic crosses. Both the triple mutant *f1 f3 PID-OE* and the double mutants *F1DN PID-OE* and *F3DN PID-OE* showed stronger phenotypes than their parental lines,

such as shorter roots and smaller cotyledons (Figure 8C). We also introduced the *pid* mutation (*pid-14*; Huang et al., 2010) into the *f1 f3* background. Since the homozygotes of both *pid* (Dhonukshe et al., 2010) and *f1 f3* are infertile, we used F2 seedlings of *pid f1 f3* for phenotyping. In *pid^{+/-}* (*pid* is heterozygous) populations, 12% (*n* = 98) of seedlings had three cotyledons, consistent with the previous observations of *pid-14* (Dhonukshe et al., 2010), while in *pid^{+/-} f1^{+/-} f3^{+/-}* (*pid*, *f1*, and *f3* are all heterozygous) populations, we observed that only 6.5% (*n* = 836) of seedlings had three cotyledons (Figure 8D). These data suggest that *f1 f3* has a dosage effect on the cotyledon phenotypes of *pid* mutants and that *f1 f3* can attenuate the *pid* cotyledon phenotypes. These data together suggest that *FyPP1* and *FyPP3* act antagonistically with *PID* to regulate plant development.

Several previous studies reported a role for *PP2AAs* (*PP2AA1/RCN1*, *A2*, and *A3* proteins) in regulating *PIN* phosphorylation, polar localization and auxin transport (Rashotte et al., 2001; Michniewicz et al., 2007); however, the role of putative catalytic subunits of *PP2A* (*PP2Ac*) in regulating *PIN* protein phosphorylation and auxin transport has not been demonstrated. The *Arabidopsis* genome contains five genes encoding the putative *c* subunits of *PP2A* (*PP2Ac1-5*), and presumably these genes have redundant functions in regulating plant development. It

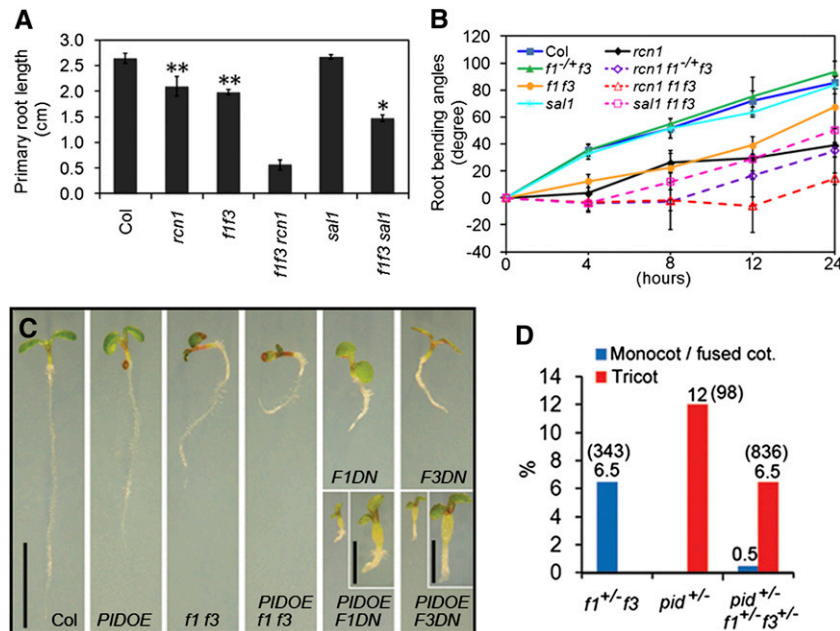


Figure 8. Genetic Interactions among Various Subunits of PP6 or between PP6 and PID.

(A) The *rcn1 f1 f3* and *sal1 f1 f3* triple mutants had shorter primary roots than their parental lines. Error bars represent \pm SE. Asterisks indicate levels of statistical significance as determined by Student's *t* test: **P* < 0.01 versus *f1 f3* and ***P* < 0.001 versus Col, *n* \geq 20.

(B) The triple mutants of *rcn1 f1^{+/-} f3*, *rcn1 f1 f3*, and *sal1 f1 f3* were less sensitive to gravistimulation than their parental lines at various time points after reorientation (4, 8, 12, and 24 h). Error bars represent \pm SE; *n* = 20.

(C) *PID-OE* significantly enhances the root phenotypes of *f1 f3*, *F1DN*, and *F3DN* mutants. Enlarged views of the double mutants *F1DN PIDOE* and *F3DN PIDOE* seedlings are shown at the top of the corresponding panels. Bars = 1 cm; bars = 0.2 cm for the enlarged views.

(D) *f1 f3* mutations attenuate the cotyledon (cot.) phenotypes of *pid* mutant. The phenotyped population of each genotype is shown in parentheses. The percentage of each phenotype to the total population is shown at the top of the bar.

[See online article for color version of this figure.]

was reported that the first Asp (D) residue in the conserved GDxVD motif of the PP2Ac N-terminal is critical for the phosphatase activity (Ogris et al., 1999; see Supplemental Figure 1 online). To investigate the role of PP2Ac subunits in regulating auxin transport, we generated an inactive mutant form of PP2Ac4 by mutating this active Asp into Asn (PP2Ac4^{D89N}; Ogris et al., 1999), mimicking the FyPP1^{D81N} and FyPP3^{D81N} mutant forms. We generated transgenic *Arabidopsis* plants that overexpress wild-type PP2Ac4 (35S:YFP-PP2Ac4/Col; hereafter, C4OE) or mutated PP2Ac4^{D89N} (35S:YFP-PP2Ac4^{D89N}/Col; hereafter, C4DN) (see Supplemental Figure 14 online). Notably, neither C4OE nor C4DN seedlings showed obvious phenotypic changes compared with Col seedling, in sharp contrast with the drastic phenotypic changes observed in F1DN or F3DN seedlings (see Supplemental Figures 14B and 14C online). These observations suggest that the putative C subunits of PP2A may only play a minor role, if any, in regulating auxin transport-dependent plant development.

DISCUSSION

In this study, we collected several lines of evidence supporting the claim that FyPP1/FyPP3, SAL, and PP2AAs proteins form a PP6 holoenzyme that plays a major role in regulating PIN phosphorylation, polar targeting, auxin transport, and diverse plant developmental processes. First, based on cation requirement, FyPP1 and FyPP3 proteins belong to PP6c, as they require Fe²⁺ or Zn²⁺ for their activity (Kim et al., 2002; Farkas et al., 2007; this study), whereas PP2A activity does not need metal ion (Wang et al., 2007). Second, FyPP1/3, SAL, and PP2AA proteins (RCN1, A2, and A3) physically interact with each other as demonstrated by a suite of Y2H, in vivo coimmunoprecipitation, and gel filtration assays. Third, FyPP1/3, SAL, and PP2AA proteins physically interact with a subset of PIN proteins, and the strength of their interaction appears to be regulated by the phosphorylation status of PIN proteins. Fourth, the phosphorylated PIN proteins overaccumulate in the *f1 f3* double mutants and *ARS2* transgenic lines. Fifth, the *f1 f3* double mutants and the *F3Ri/f1* lines after ethanol induction displayed phenotypes similar to *pp2aa* higher-order mutants or PP2AA *amiRNA* transgenic plants, including defective root development, failure of tissue patterning, and enhanced basipetal auxin transport in the roots (Rashotte et al., 2001; Zhou et al., 2004; Michniewicz et al., 2007), suggesting that FyPPs, SAL genes, and PP2AAs have comparable roles in regulating auxin transport and plant development. Sixth, we observed a basal-to-apical shift of PIN1 localization in the stele cells and a basal-to-apical shift of PIN2 localization in the cortical cells of *f1 f3*, F1DN, and F3DN roots, as previously observed in the gain-of-function *PID*, *WAG1*, and *WAG2* lines (Friml et al., 2004; Dhonukshe et al., 2010). Seventh, increased basipetal auxin transport was observed in the roots of *f1 f3* double mutants and F1DN and F3DN mutants. Eighth, we observed an antagonistic role of PID and PP6 in regulating plant development. These observations together provide strong evidence for a model in which PP6-mediated dephosphorylation promotes basal targeting of PIN proteins, while PID-dependent phosphorylation promotes apical PIN localization and subsequently

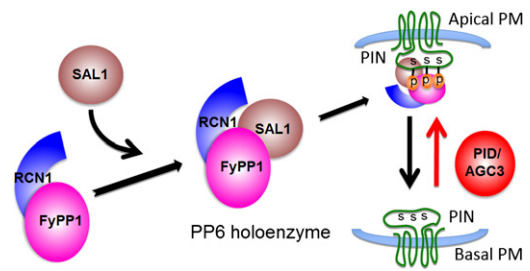


Figure 9. A Model Showing PP6 Heterotrimeric Holoenzyme Assembly and the Antagonistic Functions of PP6 and PID/AGC3 Kinase in Mediating PIN Phosphorylation and Polar Targeting.

The A subunit (RCN1) interacts with the N-terminal of the catalytic C subunit (FyPP1 or FyPP3) to form the PP6 core dimer (PP6_D). Proper function and regulation of PP6 is achieved by the association of SAL1, the regulatory B subunit, with the N terminus of the catalytic C subunit within the PP6_D, resulting in the assembly of PP6 heterotrimeric holoenzyme that may specifically interact with and dephosphorylate the conserved Ser residues (S) in the TPRxS(N/S) motifs of PIN proteins in the HLs to regulate PIN basal localization. By contrast, the Ser/Thr AGC3 kinase PID may phosphorylate PIN proteins at these sites to regulate PIN apical localization. p, phosphate; PM, plasma membrane.

regulates polar auxin transport and plant development (Figure 9). Consistent with our conclusions, a recent study also reported a role for FyPP1 in regulating the interdigitated expansion pattern of leaf epidermis cells by modulating PIN1 localization (Li et al., 2011).

It is notable that several previous studies have implied that the PP2A phosphatase is the major phosphatase regulating PIN phosphorylation and auxin transport. However, these studies are all based on the functional characterization of PP2AA proteins (the type A regulatory subunits; Rashotte et al., 2001; Michniewicz et al., 2007) or FyPP1 (the catalytic subunit; Li et al., 2011) in isolation. In this study, we first provided biochemical evidence that FyPP1 and FyPP3 function as the catalytic subunits of PP6, rather than PP2A, based on their ion requirement. Second, we showed that the PP2AA proteins (RCN1 and A3) could physically interact with FyPP1/FyPP3 and SAL proteins (the B regulatory subunits of PP6). Thus, the PP2AA proteins are most likely promiscuous and can participate in the assembly of both PP2A and PP6 holoenzymes. Third, we showed that there is a synergistic interaction among FyPP1 (or 3) (catalytic subunit), RCN1 (PP2AA1), and SAL1 in regulating plant development. Fourth, transgenic lines overexpressing a dominant-negative form of PP2Ac4^{D89N} did not show obvious phenotypic changes at the seedling stage, in contrast with the drastic phenotypic changes observed in F1DN or F3DN seedlings, suggesting that PP6, rather than PP2A, is the primary phosphatase that regulates auxin transport-dependent plant developmental processes. Our results also argue for the importance of characterizing the holoenzyme complex rather than considering the subunits in isolation in functional studies of PP2A or PP2A-like phosphatases.

Regulation by reversible phosphorylation of cell polarity proteins has also been reported to be crucial for apical-basal polarity in epithelial cells, for planar cell polarity, and for neuronal

polarization and axon growth in animals (Krahn et al., 2009; Amato et al., 2011; Gao et al., 2011). For example, the phosphorylation status of immunoglobulin receptors and Baz proteins has been shown to be crucial for their proper localization in mammalian epithelial cells and photoreceptor cells (Casanova et al., 1990; Nam et al., 2007), respectively. However, two major differences became evident concerning PP6 composition and cell polarity protein localization control in animals and plants. First, PP6 is composed of PP6c, a SAPS domain protein (PP6R), and an ankyrin repeat protein in animals (Stefansson et al., 2008), while we show here in *Arabidopsis* (and probably other plants) that PP6 is composed of FyPP1 (or 3), RCN1, and SAL1 proteins and thus represents a novel PP2A-like (including PP2A, PP4, and PP6) phosphatase holoenzyme identified in plants. Second, PP2A has been shown to play a major role in regulating cell polarity protein localization in *Drosophila melanogaster* (Nam et al., 2007; Krahn et al., 2009), while PP6 was shown to have broad functions in cell development in mammals, including cell cycle regulation, inflammatory responses, tumor necrosis factor signaling and DNA damage repair (Bastians and Ponstingl, 1996; Kajino et al., 2006; Douglas et al., 2010). Here, we show that in plants, PP6, rather than PP2A, plays a primary role in regulating PIN protein dephosphorylation, PIN polarization, and auxin transport. Thus, functional divergence among PP2A-like phosphatases (Moorhead et al., 2007) in regulating cell polarity proteins likely occurred during the evolution of plants and animals. Further dissection of the functional relationships between the multigene families of PP6 and their substrates (Farkas et al., 2007; Wang et al., 2007) in different tissues/developmental stages/in response to different external signals will ultimately lead to insights into pattern formation and organogenesis in plants.

METHODS

Plant Materials and Growth Conditions

The T-DNA insertion mutants of *fyp1* (or *f1*, CS874166), *fyp3* (or *f3*, CS877364), *rcn1-6* (SALK_059903; Blakeslee et al., 2008), *sal1* (SALK_035181), *sal2* (C3806869), *sal3* (SALK_039664), *sal4* (SALK_144179), and *pid-14* (SALK_049736) were ordered from the Salk Institute. The T-DNA insertions of *f1*, *f3*, *rcn1-6*, *sal1*, *sal2*, *sal3*, *sal4*, and *pid-14* were confirmed by PCR/sequencing; the homozygotes were identified by genotyping and further confirmed by RT-PCR expression analysis. Primers are listed in Supplemental Table 1 online. The *PIN2pro:PIN2-GFP* reporter line and *DR5:GUS* were reported previously (Xu and Scheres, 2005; Ulmasov et al., 1997). The *35S:PID-GFP* transgenic line was generated in Yunde Zhao's laboratory (Y. Zhao and G. Qin, unpublished data).

Seeds were surface sterilized with 30% bleach and 0.02% Triton X-100 for 15 min, washed with sterile distilled water four times, imbibed for 4 d at 4°C in the dark, germinated on 15-cm square Petri dishes containing Murashige and Skoog (MS) medium (0.8% agar, 1× MS salts, 1.5% Suc, and 0.5 g/L MES, pH 5.7) and grown in a plant growth chamber at 22°C.

Constructs and Transgenic Lines

For plant transformation, full-length *FyPP1*, *FyPP3*, *SAL1*, and *PP2Ac4* cDNAs were obtained by RT-PCR with F1-F1/R1, F3-F1/R1, SAL-F/R, and C4-F/R primers, respectively, and cloned into the pGEM T-Easy

vector to generate pGEM-*FyPP1*, pGEM-*FyPP3*, and pGEM-*PP2Ac4* plasmids or into the pJET1.2 vector (Fermentas) to generate pJET-*SAL1*. *FyPP1* and *PP2Ac4* were released from pGEM-*FyPP1* or pGEM-*PP2Ac4* by *Bam*HI and *Xho*I digestion, respectively. *FyPP3* was released from the pGEM-*FyPP3* plasmid by *Bgl*II and *Xho*I digestion. These fragments were inserted into the pSAT6-EYFP-C1 vector to produce pSAT6-YFP-*FyPP1*, pSAT6-YFP-*FyPP3*, and pSAT6-YFP-*PP2Ac4* plasmids, respectively. *SAL1* was released from pJET-*SAL1* by *Eco*RI and *Sal*I digestion and cloned into pSAT6-3HA (Park et al., 2008) to produce pSAT6-*SAL1-3HA*. The expression cassettes 2X35S:EYFP-*FyPP1*, 2X35S:EYFP-*FyPP3*, 2X35S:EYFP-*PP2Ac4*, and 2X35S:*SAL1-3HA* were released from pSAT6-YFP-*FyPP1*, pSAT6-YFP-*FyPP3*, pSAT6-YFP-*PP2Ac4*, and pSAT6-*SAL1-3HA* by *Pi*-*Psp*I digestion and then inserted into the pRCS2-*Bar*-OCS binary vector (Tzfira et al., 2005) to generate pRCS2(*Bar*)-YFP-*FyPP1*, pRCS2(*Bar*)-YFP-*FyPP3*, and pRCS2(*Bar*)-YFP-*PP2Ac4* plasmids or inserted into pRCS2-*Kan*-OCS to generate pRCS2(*Kan*)-*SAL1-3HA*. The *D81N* mutations in *FyPP1*/*FyPP3* and the *D89N* mutation in *PP2Ac4* were generated with the primers F1DN-F/R, F3DN-F/R, and C4DN-F/R, and the full-length cDNA fragments containing the mutations were cloned into the pGEM T-Easy vector to generate pGEM-*FyPP1*^{*D81N*}, pGEM-*FyPP3*^{*D81N*}, and pGEM-*PP2Ac4*^{*D89N*} plasmids, respectively. Using a similar strategy, the expression cassettes 2X35S:EYFP-*FyPP1*^{*D81N*}, 2X35S:EYFP-*FyPP3*^{*D81N*}, 2X35S:EYFP-*PP2Ac4*, and 2X35S:EYFP-*PP2Ac4*^{*D89N*} were inserted into the pRCS2-OCS binary vector to generate the pRCS2 (*hpt*)-YFP-*FyPP1*^{*D81N*}, pRCS2 (*hpt*)-YFP-*FyPP3*^{*D81N*}, pRCS2 (*Bar*)-YFP-*PP2Ac4*, and pRCS2 (*Bar*)-YFP-*PP2Ac4*^{*D89N*} plasmids, respectively. The *FyPP1* and *FyPP3* promoters were obtained by PCR with the primers F1p-F/R and F3p-F/R using *Arabidopsis thaliana* genomic DNA as the template and cloned into the pGEM T-Easy vector to generate the pGEM-*FyPP1pro* and pGEM-*FyPP3pro* plasmids, respectively. The *FyPP1pro* and *FyPP3pro* inserts were then released from pGEM-*FyPP1p* and pGEM-*FyPP3p* by digestion with *Eco*RI and *Nco*I and cloned into the pCAMBIA 3301 vector to generate the pCAMBIA-*FyPP1pro:GUS* and pCAMBIA-*FyPP3pro:GUS* plasmids, respectively. The *FyPP3* fragment (221 to 540) was amplified from pGEM-*FyPP3* with F3Ri-F1/R, digested by *Xho*I and *Kpn*I, and then inserted into the pHANNIBAL vector (Wesley et al., 2001) to generate pHAN-*FyPP3ia*. The same *FyPP3* fragment was amplified with F3Ri-F2/R and digested by *Bam*HI and *Cla*I and then inserted into pHAN-*FyPP3ia* to generate pHAN-*FyPP3RNAi*. The *FyPP3RNAi* fragment was released from pHAN-*FyPP3RNAi* by *Eco*RI and *Sal*I digestion and then inserted into pZM104 (gift from Eric Lam, Rutgers, The State University of New Jersey) to generate the binary vector *AlcA-AlcR:FyPP3RNAi*. amiRNA of *SAL* genes (*amiR-SAL*) was designed and the primers for amplifying the microRNA were generated with WMD3 (<http://wmd3.weigelworld.org/cgi-bin/webapp.cgi>; Schwab et al., 2006). Finally, *amiR-SAL* was inserted into pZM104 to generate the binary vector *AlcA-AlcR:amiR-SAL*. All fragments were confirmed by sequencing before cloning into the binary vectors. Various binary vectors were then introduced into *Agrobacterium tumefaciens* strain GV3101 and transformed into *Arabidopsis* Col-0 ecotype or designed mutant backgrounds using the flower dip method (Clough and Bent, 1998). Positive transformants were selected on MS plates containing the appropriate antibiotics.

For LCI assays, full-length cDNAs of *FyPP1* and *FyPP3* were released from pGEM-*FyPP1* and pGEM-*FyPP3* by digestion with *Kpn*I and *Xho*I; *SAL1* was released from pJET-*SAL1* by digestion with *Kpn*I and *Sal*I. Full-length cDNAs of *PIN1*, *PIN4*, *SAL4*, *AUX1*, and *RCN1* and the coding regions of *PIN1HL*, *PIN2HL*, and *PIN3HL* were obtained by RT-PCR with the primers PIN1-F/R, PIN4-F/R, SAL4-F/R, AUX1-F/R, RCN1-F/R, P1HL-F/R, P2HL-F/R, and P3HL-F/R, respectively, and then cloned into the pJET1.2 vector to generate pJET-*PIN1*, pJET-*PIN4*, pJET-*SAL4*, pJET-*AUX1*, pJET-*RCN1*, pJET-*PIN1HL*, pJET-*PIN2HL*, and pJET-*PIN3HL* plasmids, respectively. All fragments were confirmed by sequencing.

PIN1 and *PIN1HL* were released from pJET-*PIN1* and pJET-*PIN1HL* digested with *KpnI* and *Sall*, respectively; *PIN2HL*, *PIN4*, *PIN3HL*, *AUX1*, *RCN1*, and *SAL4* were released from pJET-*PIN2HL*, pJET-*PIN4*, pJET-*PIN3HL*, pJET-*AUX1*, pJET-*RCN1*, and pJET-*SAL4* by *KpnI* and *XhoI* digestion, respectively. These fragments were cloned into the pCAMBIA1300-*cLUC* and -*nLUC* vectors (H. Chen et al., 2008) to generate pCAMBIA-*FyPP1-nLUC*, pCAMBIA-*FyPP3-nLUC*, pCAMBIA-*PIN1-nLUC*, pCAMBIA-*PIN4-nLUC*, pCAMBIA-*SAL1-nLUC*, pCAMBIA-*SAL4-nLUC*, pCAMBIA-*AUX1-nLUC*, pCAMBIA-*RCN1-nLUC*, pCAMBIA-*PIN1HL-nLUC*, pCAMBIA-*PIN2HL-nLUC*, pCAMBIA-*PIN3HL-nLUC*, pCAMBIA-*cLUC-FyPP1*, pCAMBIA-*cLUC-FyPP3*, pCAMBIA-*cLUC-PIN1*, pCAMBIA-*cLUC-PIN4*, pCAMBIA-*cLUC-SAL1*, pCAMBIA-*cLUC-SAL4*, pCAMBIA-*cLUC-AUX1*, pCAMBIA-*cLUC-RCN1*, pCAMBIA-*cLUC-PIN1HL*, pCAMBIA-*cLUC-PIN2HL*, and pCAMBIA-*cLUC-PIN3HL*, respectively.

For recombinant protein expression, a fragment encoding *PIN2HL* was released from pJET-*PIN2HL* by digestion with *EcoRI* and *XhoI* and inserted into the pET28a vector to generate the pET28-*HIS-PIN2HL* plasmid. Full-length cDNAs of *FyPP3*, *FyPP3^{DB1N}*, *PP2Ac4*, and *PP2Ac4^{DB9N}* were released from the pGEM-*FyPP3*, pGEM-*FyPP3^{DB1N}*, pGEM-*PP2Ac4*, and pGEM-*PP2Ac4^{DB9N}* plasmids by digestion with *EcoRI* and *XhoI* and then inserted into the pGEX 4T-1 vector to produce pGEX-*GST-FyPP3*, pGEX-*GST-FyPP3^{DB1N}*, pGEX-*GST-PP2Ac4*, and pGEX-*GST-PP2Ac4^{DB9N}* plasmids, respectively.

For Y2H assays, cDNA fragments encoding NT49 (the first 49 amino acids at the N-terminal region), the catalytic domain (CD; the region from amino acid 50 to amino acid 277), and CT287 (the C-terminal region, obtained by deleting the first 49 amino acids at the N terminus) of *FyPP1* were amplified by PCR using pGEM-*FyPP1* as the template with the primers F1-F2/F1NT-R, F1CD-F/R and F1CT-F/F1-R1. The full-length cDNA of *PP2AA3* was obtained by RT-PCR with primers A3-F/R. The *PIN1HL* phosphorylation mimic mutant (*PIN1HL*, D3) and the *PIN1HL* dephosphorylation mimic mutant (*PIN1HL*, A3) were generated with the primers P1HLD1-F/R, P1HLD2-F/R, and P1HLD3-F/R and P1HLA1-F/R, P1HLA2-F/R, and P1HLA3-F/R, respectively. The *PIN2HL* phosphorylation mimic mutant (*PIN2HL*, D3) and the *PIN2HL* dephosphorylation mimic mutant (*PIN2HL*, A3) were generated with the primers P2HLD1-F/R, P2HLD2-F/R and P2HLD3-F/R and P2HLA1-F/R, P2HLA2-F/R, and P2HLA3-F/R, respectively. All of these fragments were then inserted into the pJET1.2 vector to generate pJET-*NT49*, pJET-*CD*, pJET-*CT287*, pJET-*PP2AA3*, pJET-*PIN1HL(D3)*, pJET-*PIN1HL(A3)*, pJET-*PIN2HL(D3)*, and pJET-*PIN2HL(A3)*, respectively. *NT49*, *CD*, *CT287*, *FyPP1*, *RCN1*, and *PP2A A3* were released by *EcoRI* and *XhoI* digestion from pJET-*NT49*, pJET-*CD*, pJET-*CT287*, pGEM-*FyPP1*, pJET-*RCN1*, and pJET-*PP2AA3*; *SAL1*, *PIN1HL*, *PIN1HL*, D3, *PIN1HL*, A3, *PIN2HL*, D3, and *PIN2HL*, A3 were released from the corresponding pJET plasmids by digestion with *EcoRI* and *Sall*. All released fragments were inserted into the pEG202 and pJG4.5 vectors (Yang et al., 2005) to generate fusions with LexA DNA binding domain or B42 acidic activator, respectively. For yeast three-hybrid assays, *FyPP1* was released by *KpnI* and *XhoI* from pGEM-*FyPP1* and inserted into the pGAD-T7 vector digested with *KpnI* and *XhoI* to generate pGAD-*FyPP1*.

For the coimmunoprecipitation assays, full-length *FyPP1* cDNA was amplified with F1-F2/R2 primers using pGEM-*FyPP1* plasmid DNA as template and digested with *EcoRI* and *Sall*, and the fragment was inserted into the pSAT6-3HA vector to generate the pSAT6-*FyPP1-3HA* plasmid. The *FyPP1-3HA* coding region was then released from pSAT6-*FyPP1-3HA* by digestion with *SacI* and *KpnI*, and the fragment was inserted into the pCAMBIA3301 vector to produce the pCAMBIA-*FyPP1-3HA* plasmid. *PIN2HL* was released from pJET-*PIN2HL* by *EcoRI* and *XhoI* and inserted into pSAT6-3HA vector to generate the pSAT6-*PIN2HL-3HA* plasmid. pCAMBIA-*PIN2HL-3HA* plasmid was generated using the same strategy as for the pCAMBIA-*FyPP1-3HA* plasmid. *FyPP1*, *SAL1*, and *RCN1* were

amplified from pGEM-*FyPP1*, pJET-*SAL1*, and pJET-*RCN1* with *FyPP1-F3/R3*, *SAL1-F2/R2*, and *RCN1-F2/R2*, respectively, digested by *BamHI* and *SpeI*, and then inserted into pCAMBIA-*Myc* (from Fang Chen, Yale University) to generate pCAMBIA-*Myc-FyPP1*, pCAMBIA-*Myc-SAL1*, and pCAMBIA-*Myc-RCN1*. Primers are listed in Supplemental Table 1 online.

In Vitro Ser/Thr Protein Phosphatase Activity Assays

Recombinant proteins GST-*FyPP3* and GST-*FyPP3^{DB1N}* were expressed in *Escherichia coli* strain BL21 and purified as described previously (Park et al., 2008). The activity of the phosphatases (GST-*FyPP3*, GST-*FyPP3^{DB1N}*, GST-*PP2Ac4*, and GST-*PP2Ac4^{DB9N}*) was measured using a nonradioactive molybdate dye-based phosphatase assay kit (Promega) according to the manufacturer's recommendations. A synthetic phosphopeptide, RRA[pT]VA, was used as the substrate. The reaction mixture (50 μ L) contained PP2A buffer with or without various cations (Zn^{2+} , Fe^{2+} , Mg^{2+} , and Ca^{2+}), 100 μ M phosphopeptide substrate, and 0.2 μ g phosphatase. All buffers and cations were prepared in phosphate-free water. Okadaic acid was used as a phosphatase inhibitor. The reactions were incubated at 37°C for 45 min and then stopped by adding 50 μ L molybdate dye-additive mixture. Color was developed by incubating the mixture for 30 min at room temperature. A standard curve for absorbance at 600 nm was prepared using 0, 100, 200, 500, 1000, and 2000 pmol inorganic phosphate solutions. The phosphate released by the samples was then determined by extrapolating their A_{600} against this standard curve.

Auxin Transport Assays

Auxin transport was measured according to a protocol previously described (Lewis and Muday, 2009). Briefly, seedlings were grown vertically to 5 DAG and then transferred to assay plates with or without 10 μ M NPA to grow for more than 1 h before starting the assay. Then, 100 nM of 3H -IAA (American Radiochemical) was prepared in 1.25% agar (Sigma-Aldrich; type M) solution at 50°C, and the agar droplets (10 μ L) were dispensed into a Petri dish, allowing them to solidify for 30 min in the dark at room temperature. The agar droplet was placed just under the root tip with an overlap of 0.5 mm. The plants were then incubated with the auxin source in darkness and grown vertically for 6 h at room temperature. For quantification of 3H -IAA transport, a 5-mm section of root tip 2 mm away from the auxin application site was cut for scintillation counting (Beckman; LS6500). The amount of auxin transported was then calculated according to the formula described in the protocols.

In Vitro Phosphorylation Assays

Recombinant HIS:*PIN2HL* was expressed in *E. coli* strain BL21 and purified using Ni²⁺-nitrilotriacetic acid resin according to the manufacturer's instructions (Invitrogen). In vitro kinase assays with plant extracts were performed essentially as described previously (Michniewicz et al., 2007) with a few modifications. Seedlings were harvested into liquid N₂. Total proteins were extracted with 1 \times kinase buffer (25 mM Tris-HCl, pH 7.5, 1 mM DTT, and 5 mM MgCl₂), plus 1 \times protease inhibitor and 1 mM PMSF. Two micrograms of HIS:*PIN2HL* protein and 25 μ g of plant seedling extracts were mixed in 1 \times kinase buffer, 1 \times protease inhibitor, 1 mM PMSF, and 1 \times ATP solution (100 μ M ATP and 1 μ Ci [γ -³²P]ATP) in a total volume of 50 μ L. The reactions were incubated at 30°C for 30 min and then stopped by adding 5X loading buffer and boiling for 5 min. Products were separated by electrophoresis through 12% acrylamide gels, and the gels were stained, dried, and then visualized by exposure to X-ray films.

In Vivo Phosphorylation Assays

Arabidopsis seedlings harboring *PIN2pro:PIN2-GFP* in Col and *f1 f3* backgrounds were grown to 6 DAG, and then the roots of these seedlings were harvested. The membrane protein extraction was performed as previously described (Abas and Luschnig, 2010), except that the protein phosphatase inhibitors were excluded from the extraction buffer. The membrane fractions were eventually solubilized in 0.1% Brij35 and preheated at 65°C for 10 min to inactivate the endogenous enzymes. Membrane fractions were subjected to λ -phosphatase treatment as described previously (Michniewicz et al., 2007) with a few modifications. The membrane fraction from the Col background was added to $1 \times \text{Mn}^{2+}$ (Sigma-Aldrich) and $1 \times \lambda$ -phosphatase buffer (Sigma-Aldrich) in a total volume of 50 μL . After adding $1 \times \lambda$ -phosphatase buffer to the membrane fraction from *f1 f3* mutants, three treatments were performed in a volume of 50 μL : (1) plus $1 \times \text{Mn}^{2+}$, (2) plus $1 \times \text{Mn}^{2+}$ and 200 units of λ -phosphatase (Sigma-Aldrich), (3) plus $1 \times \text{Mn}^{2+}$, 200 units of λ -phosphatase and phosphatase inhibitors (20 mM EDTA, 13 mM EGTA, 40 mM β -glycerolphosphate, 0.5 mM sodium orthovanadate, 10 nM okadaic acid, and 50 mM sodium fluoride). All samples were incubated at 30°C for 20 min. The reactions were stopped by adding $2 \times$ sample buffer (4% SDS, 250 mM Tris-HCl, pH 6.8, 80 mM dithioerythritol, and 40% glycerol) and heated. Samples were separated as described (Abas and Luschnig, 2010) and probed with GFP antibodies (Invitrogen; 1:1000). The second antibody, goat anti-rabbit IgG peroxidase antibody (Sigma-Aldrich), was used at 1:10,000. Detection was performed with the ECL Plus Western Blotting Detection System (GE Healthcare).

LCI Assays

The LCI assays were performed as previously described (H. Chen et al., 2008). All LUC^C and LUC^N fusions were introduced into the *Agrobacterium* strain GV2260. *Nicotiana benthamiana* leaves were infiltrated with the appropriate bacterial strains and the plants were incubated in constant light at room temperature for 3 d before harvesting. The luciferase activity was then determined using a Xenogen IVIS Spectrum imaging system and quantified with Living Image software (Caliper).

BiFC Assay

The vectors for BiFC assays were derived from pSY728, pSY735, pSY736, and pSY738 vectors, as described previously (Bracha-Drori et al., 2004; Shen et al., 2009). The coding sequence of *FyPP3*, *PIN1*, and *PIN2* were amplified by PCR and cloned into the pSY vectors containing either the N-terminal (1 to 155 amino acids) or C-terminal (156 to 239 amino acid) regions of the YFP fluorescent protein (YFP^N and YFP^C). Particle bombardment of possible pairwise combinations of plasmids and culture of the onion (*Allium cepa*) epidermal cells after bombardment were performed as described previously (Shen et al., 2009). YFP fluorescence was observed with a Carl Zeiss LSM510 confocal microscope.

Immunolocalization Assays

Indirect immunofluorescence staining was performed with the InSituPro robot (Intavis) according to the described protocol (Sauer et al., 2006). Antibodies and final dilutions were as follows: rabbit anti-PIN1 (Paciorek et al., 2005) 1:1000; rabbit anti-PIN2 (generously provided by C. Luschnig) 1:1000; and Cy3 anti-rabbit (Sigma-Aldrich), 1:600. Imaging was performed on a confocal laser scanning microscope. Basal localization was defined as the localization of PIN proteins to the basal side (rootward, lower) of the root cells; apical localization was defined as the localization of PIN proteins to the apical side (shootward, upper) of the root cells, while apolar localization had localization of PINs other than basal or apical, including PIN localization with lateral, basal/lateral, or apical/lateral signals.

GUS Histochemistry

The seedlings of *DR5:GUS* in *FyPP1pro:GUS* and *FyPP3pro:GUS* transgenic backgrounds were submerged in GUS staining solution [50 mM sodium phosphate, pH 7.0, 0.5% Triton X-100, 5 mM EDTA, 0.5 mM K₃Fe(CN)₆, 0.5 mM K₄Fe(CN)₆, and 2 mM 5-bromo-4-chloro-3-indolyl glucuronide] at 37°C for 0.5 h (for *DR5:GUS*) or 1.5 h (for *FyPP1pro:GUS* and *FyPP3pro:GUS*), cleared and fixed with acidic acid/alcohol (6:1), mounted with the mixture of chloral hydrate/distilled water/glycerol (8:3:0.5) and observed with differential interference contrast optics (Leica DM5500).

Y2H Assays

Y2H assays were performed as previously described (Yang et al., 2005). Briefly, pEG vectors were cotransformed with the LacZ reporter (p8op-lacZ) into the yeast strain EGY48, and positive clones were selected on His⁻Ura⁻ dropout media, while pJG vectors were transformed into the yeast strain Y864 and positive clones were selected on Trp⁻ dropout media. Strains containing the various pEG and pJG constructs were mated pairwise and screened on His⁻Ura⁻Trp⁻ triple dropout media. For yeast three-hybrid assays, pEG vectors were cotransformed with the LacZ reporter (p8op-lacZ) into the yeast strain EGY48, and positive clones were selected on His⁻Ura⁻ dropout media, while pJG vectors and pGAD vectors were transformed into the yeast strain Y864 and positive clones were selected on Leu⁻Trp⁻ dropout media. Strains containing various pEG, LacZ, pGAD, and pJG constructs were mated pairwise and screened on Leu⁻His⁻Ura⁻Trp⁻ dropout media. Color development was performed on His⁻Ura⁻Trp⁻ dropout (for Y2H) or Leu⁻His⁻Ura⁻Trp⁻ dropout (for yeast three-hybrid assays) plates supplemented with $1 \times$ buffered salt, 2% Gal, 1% raffinose, and 0.08 mg/mL X-Gal. Liquid assays were performed using the Yeast β -Galactosidase Assay Kit (Pierce) according to the manufacturer's instructions.

Coimmunoprecipitation and Immunoblot Assays

Various expression vectors were introduced into the *Agrobacterium* strain GV2260. Various combinations of plasmids were coinfiltrated into tobacco (*Nicotiana tabacum*) leaves as previously described (H. Chen et al., 2008) and grown for 3 d. Protein extraction and coimmunoprecipitation were performed as described (Moffett et al., 2002). Briefly, for protein extraction, 1 g of tobacco leaves pulverized in a prechilled mortar with liquid N₂ was thawed in 2.5 mL of GTEN extraction buffer (10% glycerol, 25 mM Tris, pH 7.5, 1 mM EDTA, 150 mM NaCl, 10 mM DTT, and 2% [w/v] polyvinylpyrrolidone) and $1 \times$ protease inhibitor cocktail (Sigma-Aldrich plant protease inhibitor cocktail). Protein extracts were cleaned by centrifugation and passage through an acrylamide-based desalting matrix column (Bio-Gel P6 DG) before immunoprecipitation. IP was performed with 25 μL precleaned α -HA affinity matrix (Roche) and 1 mL desalted protein extracts in immunoprecipitation buffer (GTEN buffer, without polyvinylpyrrolidone, plus 0.15% Nonidet P-40). After immunoprecipitation, the matrix was washed four times with fresh immunoprecipitation buffer. Proteins were then released and collected by boiling the matrix in $1 \times$ SDS loading buffer for 5 min. Immunoprecipitation products were separated by electrophoresis through 10% acrylamide gels, and the target proteins were detected by protein gel blots using α -LUC (Sigma-Aldrich), α -HA, or α -Myc antibodies (Roche).

Gel Filtration Chromatography

For gel filtration analysis, 7-d-old *Arabidopsis* seedlings were extracted in a lysis buffer containing 50 mM Tris-HCl, pH 7.5, 150 mM NaCl, and 1 mM EDTA. Extracts were centrifuged at 13,000g for 15 min at 4°C and then filtered through 0.22- μm syringe filters. Superdex 200 columns (Amersham Biosciences) were used to fractionate the samples. After the

void volume was eluted, consecutive fractions (500 μ L) were collected, concentrated using Strataclean resin (Stratagene), and then analyzed by protein gel blots with α -HA (Roche) and α -GFP (Invitrogen) antibodies.

Microscopy and Confocal Observations

Root cap starch granules were stained with 1% Lugol's staining solution (Sigma-Aldrich) for 2 min at room temperature, rinsed in water, and cleared with chloral hydrate/distilled water/glycerol (8:3:0.5) and observed by differential interference contrast microscopy (Leica DM5500). To observe the root meristem structure, roots were submerged in 20 μ g/mL propidium iodide solution (Invitrogen) for 2 to 5 min at room temperature, rinsed in water, and observed with a Carl Zeiss LSM510 confocal microscope. GFP fluorescence was observed with a Carl Zeiss LSM510 confocal microscope.

Gravitropism Assays

Gravitropism assays were conducted essentially as described (Rashotte et al., 2001). Five-day-old seedlings were transferred to fresh MS plates and grown vertically for 24 h, and then the plates were reoriented 90°. The angles of new root growth were captured with a Nikon camera every 4 h over a 24-h period after reorientation. The angles were then measured by ImageJ (<http://rsb.info.nih.gov/ij/>) software. To assay root vertical growth index, seedlings were grown vertically on MS plates for 5 d. The quantification tool in ImageJ software was used to calculate the vertical growth index (VGI = vertical length/root length) (Zhang et al., 2010).

Hormonal Treatments

Hormonal treatments were performed essentially as described (Lin and Wang, 2005). Three-day-old seedlings were transferred onto assay plates (with either 2,4-D or 1-naphthaleneacetic acid) or control plates (without hormone). The primary root positions were marked. The seedlings were then grown for 4 d vertically under continuous light. New root growth was measured with a ruler. The relative root growth was then calculated by comparing the new growth on the assay plates with the new root growth on control plates. Lateral roots were observed using a dissecting microscope and counted if there was a visible primordium. For IAA treatment, after 5 d of vertical growth, seedlings harboring *DR5:GUS* in different backgrounds were transferred onto the plates with 100 μ M IAA for 18 h and then the seedlings were rinsed in water and subjected to GUS staining. For NPA treatment, the seedlings were grown on plates for 5 d and then transferred to plates with or without 0.3 μ M NPA to grow for one more day. The seedlings were then harvested for staining with Lugol's staining solution, followed by microscopy observation.

Accession Numbers

The National Center for Biotechnology Information accession numbers for the genes studied in this work are *At1g50370* (*FyPP1*), *At3g19980* (*FyPP3*), *At1g07990* (*SAL1*), *At1g30470* (*SAL2*), *At2g28360* (*SAL3*), *At3g45190* (*SAL4*), and *AT2G42500* (*PP2Ac4*). National Center for Biotechnology Information accession numbers for the proteins are *AtFyPP1*, NP_175454; *AtFyPP3*, NP_188632; *OsPP6c*, NP_001043937; *ZmPP6c*, NP_001142145; *PtPP6c*, XP_002310919; *HsPP6c*, NP_002712; *MmPP6c*, NP_077171; *CsSIT4*, CAA98609; *AtPP2Ac1*, Q07099; *AtPP2Ac2*, Q07098; *AtPP2Ac3*, P48578; *AtPP2Ac4*, Q07100; and *AtPP2Ac5*, O04951.

Supplemental Data

The following materials are available in the online version of this article.

Supplemental Figure 1. Sequence Alignment of the C Subunits of PP6 and PP2A Phosphatases.

Supplemental Figure 2. In Vitro Enzyme Activity Assay of GST-FyPP3 and GST-FyPP3^{DB1N}.

Supplemental Figure 3. Diagram of the Gene Structures and T-DNA Insertion Mutants of *FyPP1* and *FyPP3*.

Supplemental Figure 4. Roles of *FyPP1* and *FyPP3* in Cotyledon and Root Development.

Supplemental Figure 5. Characterization of the Transgenes in *F1OE*, *F3OE*, *F1DN*, and *F3DN* Transgenic Plants.

Supplemental Figure 6. Analysis of the Root Phenotypes of Plants Overexpressing *YFP-FyPP1*, *YFP-FyPP1^{DB1N}*, *YFP-FyPP*, or *YFP-FyPP3^{DB1N}*.

Supplemental Figure 7. *f1 f3*, *F1OE*, *F3OE*, and *F3DN* Plants Show Comparable Responses to Exogenous Auxin.

Supplemental Figure 8. Root Auxin Basipetal Transport in *Col* and *f1 f3* Roots Treated with NPA.

Supplemental Figure 9. Subcellular Localization of YFP-FyPP1 and YFP-FyPP3 in Root Cells.

Supplemental Figure 10. Root Phenotypes of *Col* and *F3Ri/f1* after Ethanol Treatment.

Supplemental Figure 11. Protein-Protein Interactions between FyPP3 and PIN1 or PIN2 in Onion Cells.

Supplemental Figure 12. Phenotypic Characterization of Root Development in *sal1*, *sal2*, *sal3*, *sal4*, and *SAL1-OE* Plants.

Supplemental Figure 13. Changed PIN Phosphorylation Status in *ARS2* Plants after Ethanol Induction.

Supplemental Figure 14. Comparison of the Phenotypes of *35S:YFP-PP2Ac4/Col* (*C4OE*), *35S:YFP-PP2Ac4^{DB9N}/Col* (*C4DN*), *F1DN*, and *F3DN* Plants.

Supplemental Table 1. List of the Oligonucleotides Used in This Study.

Supplemental References 1. Supplemental References for Supplemental Figure 1.

Supplemental Data Set 1. Amino Acid Sequence Alignment Used to Generate the Phylogeny Presented in Supplemental Figure 1.

ACKNOWLEDGMENTS

We thank Alison Delong (Brown University) for sharing the seeds of *RCN1pro:YFP-RCN1* lines, Tian Xu (Yale University) for providing Xenogen IVIS spectrum equipment for the LCI assay, Hong-Gu Kong (Boyce Thompson Institute for Plant Research) for the pBIN61-*GFP-3HA* vector, Eric Lam (Rutgers, The State University of New Jersey) for the pZM104 inducible binary vector, and Jian-Min Zhou (National Institute of Biological Science, Beijing) for sharing the pCAMBIA-*nLUC* and *-cLUC* vectors. We thank Chentao Lin (University of California-Los Angeles) and Zhiyong Wang (Carnegie Institute for Science, Stanford University) for critical reading and comments on the article. This work was supported by funds from National Science Foundation (MCB-1004808, IOS-0954313, and IOS-1026630 to H.W.) and the National Institutes of Health (GM47850 to X.W.D.).

AUTHOR CONTRIBUTIONS

H.W., X.W.D., J.F., J.X., and M.D. designed the research. M.D. cloned the constructs, generated the transgenic plants, established the mutants,

measured the auxin transport, performed in vitro/in vivo phosphorylation assay, in vitro phosphatase activity assay, protein–protein interaction assays, and expression analysis. C.Z. did Lugol's staining, GUS staining, and genotyping. U.K. performed immunolocalization. G.L. did the gel filtration assay. F.C. did the BiFC assay. G.Q. and Y.Z. generated the *PID-OE* transgenic lines. T.M., Q.X., M.W., W.T., and J.W. did the genotyping. M.D. and H.W. wrote the article.

Received April 2, 2012; revised May 7, 2012; accepted May 31, 2012; published June 19, 2012.

REFERENCES

- Abas, L., and Luschnig, C.** (2010). Maximum yields of microsomal-type membranes from small amounts of plant material without requiring ultracentrifugation. *Anal. Biochem.* **401**: 217–227.
- Amato, S., Liu, X., Zheng, B., Cantley, L., Rakic, P., and Man, H.Y.** (2011). AMP-activated protein kinase regulates neuronal polarization by interfering with PI 3-kinase localization. *Science* **332**: 247–251.
- Bastians, H., and Ponstingl, H.** (1996). The novel human protein serine/threonine phosphatase 6 is a functional homologue of budding yeast Sit4p and fission yeast ppe1, which are involved in cell cycle regulation. *J. Cell Sci.* **109**: 2865–2874.
- Benjamins, R., Quint, A., Weijers, D., Hooykaas, P., and Offringa, R.** (2001). The PINOID protein kinase regulates organ development in *Arabidopsis* by enhancing polar auxin transport. *Development* **128**: 4057–4067.
- Bennett, T., and Scheres, B.** (2010). Root development—two meristems for the price of one? *Curr. Top. Dev. Biol.* **91**: 67–102.
- Blakeslee, J.J. et al.** (2007). Interactions among PIN-FORMED and P-glycoprotein auxin transporters in *Arabidopsis*. *Plant Cell* **19**: 131–147.
- Blakeslee, J.J., Zhou, H.W., Heath, J.T., Skottke, K.R., Barrios, J.A., Liu, S.Y., and DeLong, A.** (2008). Specificity of RCN1-mediated protein phosphatase 2A regulation in meristem organization and stress response in roots. *Plant Physiol.* **146**: 539–553.
- Blilou, I., Xu, J., Wildwater, M., Willemsen, V., Paponov, I., Friml, J., Heidstra, R., Aida, M., Palme, K., and Scheres, B.** (2005). The PIN auxin efflux facilitator network controls growth and patterning in *Arabidopsis* roots. *Nature* **433**: 39–44.
- Bouchard, R., Bailly, A., Blakeslee, J.J., Oehring, S.C., Vincenzetti, V., Lee, O.R., Paponov, I., Palme, K., Mancuso, S., Murphy, A.S., Schulz, B., and Geisler, M.** (2006). Immunophilin-like TWISTED DWARF1 modulates auxin efflux activities of *Arabidopsis* P-glycoproteins. *J. Biol. Chem.* **281**: 30603–30612.
- Bracha-Drori, K., Shichrur, K., Katz, A., Oliva, M., Angelovici, R., Yalovsky, S., and Ohad, N.** (2004). Detection of protein-protein interactions in plants using bimolecular fluorescence complementation. *Plant J.* **40**: 419–427.
- Casanova, J.E., Breiffeld, P.P., Ross, S.A., and Mostov, K.E.** (1990). Phosphorylation of the polymeric immunoglobulin receptor required for its efficient transcytosis. *Science* **248**: 742–745.
- Chen, G.I., Tisayakorn, S., Jorgensen, C., D'Ambrosio, L.M., Goudreau, M., and Gingras, A.C.** (2008). PP4R4/KIAA1622 forms a novel stable cytosolic complex with phosphoprotein phosphatase 4. *J. Biol. Chem.* **283**: 29273–29284.
- Chen, H., Zou, Y., Shang, Y., Lin, H., Wang, Y., Cai, R., Tang, X., and Zhou, J.M.** (2008). Firefly luciferase complementation imaging assay for protein-protein interactions in plants. *Plant Physiol.* **146**: 368–376.
- Chen, R., Hilson, P., Sedbrook, J., Rosen, E., Caspar, T., and Masson, P.H.** (1998). The *Arabidopsis thaliana* AGRAVITROPIC 1 gene encodes a component of the polar-auxin-transport efflux carrier. *Proc. Natl. Acad. Sci. USA* **95**: 15112–15117.
- Christensen, S.K., Dagenais, N., Chory, J., and Weigel, D.** (2000). Regulation of auxin response by the protein kinase PINOID. *Cell* **100**: 469–478.
- Clough, S.J., and Bent, A.F.** (1998). Floral dip: A simplified method for *Agrobacterium*-mediated transformation of *Arabidopsis thaliana*. *Plant J.* **16**: 735–743.
- Dhonukshe, P., Huang, F., Galvan-Ampudia, C.S., Mähönen, A.P., Kleine-Vehn, J., Xu, J., Quint, A., Prasad, K., Friml, J., Scheres, B., and Offringa, R.** (2010). Plasma membrane-bound AGC3 kinases phosphorylate PIN auxin carriers at TPRXS(N/S) motifs to direct apical PIN recycling. *Development* **137**: 3245–3255.
- Douglas, P., Zhong, J., Ye, R., Moorhead, G.B., Xu, X., and Lees-Miller, S.P.** (2010). Protein phosphatase 6 interacts with the DNA-dependent protein kinase catalytic subunit and dephosphorylates gamma-H2AX. *Mol. Cell. Biol.* **30**: 1368–1381.
- Farkas, I., Dombrádi, V., Miskei, M., Szabados, L., and Koncz, C.** (2007). *Arabidopsis* PPP family of serine/threonine phosphatases. *Trends Plant Sci.* **12**: 169–176.
- Friml, J., Benková, E., Blilou, I., Wisniewska, J., Hamann, T., Jung, K., Woody, S., Sandberg, G., Scheres, B., Jürgens, G., and Palme, K.** (2002). AtPIN4 mediates sink-driven auxin gradients and root patterning in *Arabidopsis*. *Cell* **108**: 661–673.
- Friml, J., Vieten, A., Sauer, M., Weijers, D., Schwarz, H., Hamann, T., Offringa, R., and Jürgens, G.** (2003). Efflux-dependent auxin gradients establish the apical-basal axis of *Arabidopsis*. *Nature* **426**: 147–153.
- Friml, J. et al.** (2004). A PINOID-dependent binary switch in apical-basal PIN polar targeting directs auxin efflux. *Science* **306**: 862–865.
- Gälweiler, L., Guan, C., Müller, A., Wisman, E., Mendgen, K., Yephremov, A., and Palme, K.** (1998). Regulation of polar auxin transport by AtPIN1 in *Arabidopsis* vascular tissue. *Science* **282**: 2226–2230.
- Gao, B., Song, H., Bishop, K., Elliot, G., Garrett, L., English, M.A., Andre, P., Robinson, J., Sood, R., Minami, Y., Economides, A.N., and Yang, Y.** (2011). Wnt signaling gradients establish planar cell polarity by inducing Vangl2 phosphorylation through Ror2. *Dev. Cell* **20**: 163–176.
- Garbers, C., DeLong, A., Deruère, J., Bernasconi, P., and Söll, D.** (1996). A mutation in protein phosphatase 2A regulatory subunit A affects auxin transport in *Arabidopsis*. *EMBO J.* **15**: 2115–2124.
- Ge, L., Peer, W., Robert, S., Swarup, R., Ye, S., Prigge, M., Cohen, J.D., Friml, J., Murphy, A., Tang, D., and Estelle, M.** (2010). *Arabidopsis* ROOT UVB SENSITIVE2/WEAK AUXIN RESPONSE1 is required for polar auxin transport. *Plant Cell* **22**: 1749–1761.
- Grunewald, W., and Friml, J.** (2010). The march of the PINs: Developmental plasticity by dynamic polar targeting in plant cells. *EMBO J.* **29**: 2700–2714.
- Huang, F., Zago, M.K., Abas, L., van Marion, A., Galván-Ampudia, C.S., and Offringa, R.** (2010). Phosphorylation of conserved PIN motifs directs *Arabidopsis* PIN1 polarity and auxin transport. *Plant Cell* **22**: 1129–1142.
- Janssens, V., Longin, S., and Goris, J.** (2008). PP2A holoenzyme assembly: in cauda venenum (the sting is in the tail). *Trends Biochem. Sci.* **33**: 113–121.
- Kajino, T., Ren, H., Iemura, S., Natsume, T., Stefansson, B., Brautigan, D.L., Matsumoto, K., and Ninomiya-Tsuji, J.** (2006). Protein phosphatase 6 down-regulates TAK1 kinase activation in the IL-1 signaling pathway. *J. Biol. Chem.* **281**: 39891–39896.
- Kim, D.H., Kang, J.G., Yang, S.S., Chung, K.S., Song, P.S., and Park, C.M.** (2002). A phytochrome-associated protein phosphatase 2A modulates light signals in flowering time control in *Arabidopsis*. *Plant Cell* **14**: 3043–3056.

- Kleine-Vehn, J., Langowski, L., Wisniewska, J., Dhonukshe, P., Brewer, P.B., and Friml, J.** (2008). Cellular and molecular requirements for polar PIN targeting and transcytosis in plants. *Mol. Plant* **1**: 1056–1066.
- Krahn, M.P., Egger-Adam, D., and Wodarz, A.** (2009). PP2A antagonizes phosphorylation of Bazooka by PAR-1 to control apical-basal polarity in dividing embryonic neuroblasts. *Dev. Cell* **16**: 901–908.
- Lewis, D.R., and Muday, G.K.** (2009). Measurement of auxin transport in *Arabidopsis thaliana*. *Nat. Protoc.* **4**: 437–451.
- Li, H., Lin, D., Dhonukshe, P., Nagawa, S., Chen, D., Friml, J., Scheres, B., Guo, H., and Yang, Z.** (2011). Phosphorylation switch modulates the interdigitated pattern of PIN1 localization and cell expansion in *Arabidopsis* leaf epidermis. *Cell Res.* **21**: 970–978.
- Lin, R., and Wang, H.** (2005). Two homologous ATP-binding cassette transporter proteins, AtMDR1 and AtPGP1, regulate *Arabidopsis* photomorphogenesis and root development by mediating polar auxin transport. *Plant Physiol.* **138**: 949–964.
- Luke, M.M., Della Seta, F., Di Como, C.J., Sugimoto, H., Kobayashi, R., and Arndt, K.T.** (1996). The SAP, a new family of proteins, associate and function positively with the SIT4 phosphatase. *Mol. Cell. Biol.* **16**: 2744–2755.
- Michniewicz, M. et al.** (2007). Antagonistic regulation of PIN phosphorylation by PP2A and PINOID directs auxin flux. *Cell* **130**: 1044–1056.
- Moffett, P., Farnham, G., Peart, J., and Baulcombe, D.C.** (2002). Interaction between domains of a plant NBS-LRR protein in disease resistance-related cell death. *EMBO J.* **21**: 4511–4519.
- Moorhead, G.B., Trinkle-Mulcahy, L., and Ulke-Lemée, A.** (2007). Emerging roles of nuclear protein phosphatases. *Nat. Rev. Mol. Cell Biol.* **8**: 234–244.
- Müller, A., Guan, C., Gälweiler, L., Tänzler, P., Huijser, P., Marchant, A., Parry, G., Bennett, M., Wisman, E., and Palme, K.** (1998). AtPIN2 defines a locus of *Arabidopsis* for root gravitropism control. *EMBO J.* **17**: 6903–6911.
- Nam, S.C., Mukhopadhyay, B., and Choi, K.W.** (2007). Antagonistic functions of Par-1 kinase and protein phosphatase 2A are required for localization of Bazooka and photoreceptor morphogenesis in *Drosophila*. *Dev. Biol.* **306**: 624–635.
- Ogris, E., Mudrak, I., Mak, E., Gibson, D., and Pallas, D.C.** (1999). Catalytically inactive protein phosphatase 2A can bind to polyomavirus middle tumor antigen and support complex formation with pp60(c-src). *J. Virol.* **73**: 7390–7398.
- Paciorek, T., Zazimalová, E., Ruthardt, N., Petrásek, J., Stierhof, Y.D., Kleine-Vehn, J., Morris, D.A., Emans, N., Jürgens, G., Geldner, N., and Friml, J.** (2005). Auxin inhibits endocytosis and promotes its own efflux from cells. *Nature* **435**: 1251–1256.
- Park, H.J., Ding, L., Dai, M., Lin, R., and Wang, H.** (2008). Multisite phosphorylation of *Arabidopsis* HFR1 by casein kinase II and a plausible role in regulating its degradation rate. *J. Biol. Chem.* **283**: 23264–23273.
- Peris, C.I., Rademacher, E.H., and Weijers, D.** (2010). Green beginnings - Pattern formation in the early plant embryo. *Curr. Top. Dev. Biol.* **91**: 1–27.
- Petrásek, J. et al.** (2006). PIN proteins perform a rate-limiting function in cellular auxin efflux. *Science* **312**: 914–918.
- Rashotte, A.M., DeLong, A., and Muday, G.K.** (2001). Genetic and chemical reductions in protein phosphatase activity alter auxin transport, gravity response, and lateral root growth. *Plant Cell* **13**: 1683–1697.
- Sauer, M., Paciorek, T., Benková, E., and Friml, J.** (2006). Immunocytochemical techniques for whole-mount *in situ* protein localization in plants. *Nat. Protoc.* **1**: 98–103.
- Schlereth, A., Möller, B., Liu, W., Kientz, M., Flipse, J., Rademacher, E.H., Schmid, M., Jürgens, G., and Weijers, D.** (2010). MONOPTEROS controls embryonic root initiation by regulating a mobile transcription factor. *Nature* **464**: 913–916.
- Schwab, R., Ossowski, S., Rieger, M., Warthmann, N., and Weigel, D.** (2006). Highly specific gene silencing by artificial microRNAs in *Arabidopsis*. *Plant Cell* **18**: 1121–1133.
- Shen, Y., Zhou, Z., Feng, S., Li, J., Tan-Wilson, A., Qu, L.J., Wang, H., and Deng, X.W.** (2009). Phytochrome A mediates rapid red light-induced phosphorylation of *Arabidopsis* FAR-RED ELONGATED HYPOCOTYL1 in a low fluence response. *Plant Cell* **21**: 494–506.
- Slupe, A.M., Merrill, R.A., and Strack, S.** (2011). Determinants for substrate specificity of protein phosphatase 2A. *Enzyme Res.* **2011**: 398751.
- Stefansson, B., and Brautigan, D.L.** (2006). Protein phosphatase 6 subunit with conserved Sit4-associated protein domain targets IkkappaBepsilon. *J. Biol. Chem.* **281**: 22624–22634.
- Stefansson, B., Ohama, T., Daugherty, A.E., and Brautigan, D.L.** (2008). Protein phosphatase 6 regulatory subunits composed of ankyrin repeat domains. *Biochemistry* **47**: 1442–1451.
- Swarup, K. et al.** (2008). The auxin influx carrier LAX3 promotes lateral root emergence. *Nat. Cell Biol.* **10**: 946–954.
- Swarup, R., Kramer, E.M., Perry, P., Knox, K., Leyser, H.M., Haseloff, J., Beechster, G.T., Bhalerao, R., and Bennett, M.J.** (2005). Root gravitropism requires lateral root cap and epidermal cells for transport and response to a mobile auxin signal. *Nat. Cell Biol.* **7**: 1057–1065.
- Terasaka, K., Blakeslee, J.J., Titapiwatanakun, B., Peer, W.A., Bandyopadhyay, A., Makam, S.N., Lee, O.R., Richards, E.L., Murphy, A.S., Sato, F., and Yazaki, K.** (2005). PGP4, an ATP binding cassette P-glycoprotein, catalyzes auxin transport in *Arabidopsis thaliana* roots. *Plant Cell* **17**: 2922–2939.
- Terol, J., BARGUES, M., Carrasco, P., Pérez-Alonso, M., and Paricio, N.** (2002). Molecular characterization and evolution of the protein phosphatase 2A B' regulatory subunit family in plants. *Plant Physiol.* **129**: 808–822.
- Tzfira, T., Tian, G.W., Lacroix, B., Vyas, S., Li, J., Leitner-Dagan, Y., Krichevsky, A., Taylor, T., Vainstein, A., and Citovsky, V.** (2005). pSAT vectors: A modular series of plasmids for autofluorescent protein tagging and expression of multiple genes in plants. *Plant Mol. Biol.* **57**: 503–516.
- Ulmasov, T., Murfett, J., Hagen, G., and Guilfoyle, T.J.** (1997). Aux/IAA proteins repress expression of reporter genes containing natural and highly active synthetic auxin response elements. *Plant Cell* **9**: 1963–1971.
- Wang, H., Chevalier, D., Larue, C., Cho, S.K., and Walker, J.C.** (2007). The protein phosphatases and protein kinases of *Arabidopsis thaliana*. *The Arabidopsis Book* **5**: e0106. doi/10.1199/tab.0106.
- Wesley, S.V. et al.** (2001). Construct design for efficient, effective and high-throughput gene silencing in plants. *Plant J.* **27**: 581–590.
- Wiśniewska, J., Xu, J., Seifertová, D., Brewer, P.B., Ruzicka, K., Blilou, I., Rouquié, D., Benková, E., Scheres, B., and Friml, J.** (2006). Polar PIN localization directs auxin flow in plants. *Science* **312**: 883.
- Xu, J., and Scheres, B.** (2005). Dissection of *Arabidopsis* ADP-RIBOSYLATION FACTOR 1 function in epidermal cell polarity. *Plant Cell* **17**: 525–536.
- Yang, J., Lin, R., Sullivan, J., Hoecker, U., Liu, B., Xu, L., Deng, X.W., and Wang, H.** (2005). Light regulates COP1-mediated degradation of HFR1, a transcription factor essential for light signaling in *Arabidopsis*. *Plant Cell* **17**: 804–821.
- Zhang, J., Nodzyński, T., Pencík, A., Rolcík, J., and Friml, J.** (2010). PIN phosphorylation is sufficient to mediate PIN polarity and direct auxin transport. *Proc. Natl. Acad. Sci. USA* **107**: 918–922.
- Zhou, H.W., Nussbaumer, C., Chao, Y., and DeLong, A.** (2004). Disparate roles for the regulatory A subunit isoforms in *Arabidopsis* protein phosphatase 2A. *Plant Cell* **16**: 709–722.